The Department of Geodesy and Geoinformatics

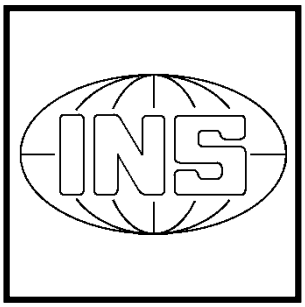

Stuttgart University

2016

editing and layout:
volker walter, markus antoni, martin metzner, aloysius wehr

Dear friends and colleagues,

It is our great pleasure to present to you this annual report[1] on the 2016 activities and academic highlights of the Department of Geodesy and Geoinformatics of the University of Stuttgart. The Department consists of the four institutes:

- Institute of Geodesy (GIS),
- Institute of Photogrammetry (ifp),
- Institute of Navigation (INS),
- Institute of Engineering Geodesy (IIGS),

and is part of the Faculty of Aerospace Engineering and Geodesy.

Research

This annual report documents our research contributions in many diverse fields of Geodesy and Geoinformatics: from satellite and physical geodesy through navigation, remote sensing, engineering surveying and telematics to photogrammetry, geographical information systems and location based services. Detailed information on projects and research output can be found in the following individual institutes' sections.

Teaching

We were able to welcome 57 new BSc students in winter term 2015/2016. The first BSc students graduated at the end of 2013. Until the end of 2016 we had in total 70 BSc graduates. The MSc program for Geodesy and Geoinformatics started with the winter term 2012. Currently 48 students are taking part in this Master of Science program and we have already 22 MSc graduates. The Diploma program has terminated on March 31 2017. All our Diploma students got their Diploma degree. Total enrolment, in both the BSc, Msc and the Diploma programs, is increasing an amounts to 238 students. Please visit our website www.geodaesie.uni-stuttgart.de for additional information on the programs.

In its 11th year of existence, our international MSc program *Geomatics Engineering* (GeoEngine) enjoys a gratifying demand. We register an enrolment of 26 students. We attract the GeoEngine student population from such diverse countries as China, Palestine, Iran, Ghana, Ecuador, Nepal, India, Canada and Japan. Please visit www.geoengine.uni-stuttgart.de for more information.

[1] A version with colour graphics is downloadable from
http://www.ifp.uni-stuttgart.de/publications/jahresberichte/jahresbericht.html

Awards and scholarships

We want to express our gratitude to our friends and sponsors, most notably:

- Verein Freunde des Studienganges Geodäsie und Geoinformatik an der Universität Stuttgart e.V. (F2GeoS),
- Microsoft company Vexcel Imaging GmbH,
- Ingenieur-Gesellschaft für Interfaces mbH (IGI),
- DVW Landesverein Baden-Württemberg,

who support our programs and our students with scholarships, awards and travel support.

Below is the list of the recipients of the 2015/16 awards and scholarships. The criterion for all prizes is academic performance; for some prizes GPA-based, for other prizes based on thesis work. Congratulations to all recipients!

Wolfgang Keller
Associate Dean (Academic)
wolfgang.keller@gis.uni-stuttgart.de

Award	**Recipient**	**Sponsor**	**Programme**
Karl-Ramsayer Preis	V. Mayer	Department of Geodesy & Geoinformatics	Geodesy & Geo-informatics
BSc Thesis Award	J. Aichinger	F2GeoS	Geodesy & Geo-informatics
MSc Thesis Award	P. Pitzer	F2GeoS	Geodesy & Geo-informatics
MS Photogrammetry / Vexcel Imaging Scholarship	P. Li S. Lakshmaiah K. Zhan L. Zhou	MS Photogrammetry / Vexcel Imaging	GEOENGINE
matching funds	C. Xu M. Kokhova R. Xia H. Li	DAAD	GEOENGINE

Institute for Engineering Geodesy

Geschwister-Scholl-Str. 24D, D-70174 Stuttgart,
Tel.: +49 711 685 84041, Fax: +49 711 685 84044
e-mail: Sekretariat@ingeo.uni-stuttgart.de or
firstname.secondname@ingeo.uni-stuttgart.de
url: http://www.uni-stuttgart.de/ingeo/

Head of Institute

Prof. Dr.-Ing. habil. Volker Schwieger

Secretary

Elke Rawe
Ute Schinzel

Emeritus

Prof. Dr.-Ing. Dr.sc.techn.h.c. Dr.h.c. Klaus Linkwitz

Scientific Staff

Dr.-Ing. Ashraf Abdallah (until 31.03.2016)	GNSS Positioning
M.Sc. Bara' Al-Mistarehi (until 31.03.2016)	Construction Process
M. Sc. Alexandra Avram (since 01.10.2016)	GNSS
M.Sc. Marko Gasparac (since 01.01.2016)	GNSS and Digital Map
M.Sc. Aiham Hassan	Monitoring
Dipl.-Ing. Patric Hindenberger (since 01.08.2016)	Location Referencing
Dipl.-Ing. Stephanie Kauker	Monitoring
Dipl.-Ing. Otto Lerke	Machine Guidance
Dr.-Ing. Martin Metzner	Engineering Geodesy
Dipl.-Ing. Annette Scheider	Kinematic Positioning
M.Sc. Pham Trung Dung	Kinematic Positioning
M.Sc. Annette Schmitt	Multi-Sensor-Systems
Dr.-Ing. Rainer Schützle (until 30.06.2016)	Location Referencing
M.Sc. Jinyue Wang	Map Matching
Dr.-Ing. Li Zhang	Monitoring

Technical Staff

Andreas Kanzler
Martin Knihs
Lars Plate

External Teaching Staff

Dipl.-Ing. Jürgen Eisenmann	Geschäftsbereichsleiter Landratsamt Ostalbkreis - Geoinformation und Landentwicklung
Dipl.-Ing. Christian Helfert	Fachdienstleiter Flurneuordnung im Landkreis Biberach
Dipl.-Math. Ulrich Völter	Geschäftsführer der Fa. Intermetric
Dr.-Ing. Thomas Wiltschko	Daimler AG, Mercedes-Benz Cars; Research and Development

General View

The Institute of Engineering Geodesy (IIGS) is directed by Prof. Dr.-Ing. habil. Volker Schwieger. It is part of the Faculty 6 „Aerospace Engineering and Geodesy“ within the University of Stuttgart. Prof. Schwieger holds the chair in „Engineering Geodesy and Geodetic Measurements“. In 2016 he was elected Dean of Faculty 6.

In addition to being a member of Faculty 6, Prof. Schwieger is co-opted to Faculty 2 „Civil and Environmental Engineering“. Furthermore, IIGS is involved in the Center for Transportation Research of the University of Stuttgart (FOVUS). So, IIGS actively continues the close collaboration with all institutes in the field of transportation, especially with those belonging to Faculty 2.

Since 2011 he is a full member of the German Geodetic Commission (Deutsche Geodätische Kommission - DGK). Furthermore, Prof. Schwieger is a member of the section „Engineering Geodesy“ within the DGK. He is head of the DVW working group 3 „Measurement Techniques and Systems“ and chairman of the FIG Commission 5 „Positioning and Measurements“ in the period from 2015 to 2018.

The institute's main tasks in education focus on geodetic and industrial measurement techniques, kinematic positioning and multi-sensor systems, statistics and error theory, engineering geodesy and monitoring, GIS-based data acquisition, and transport telematics. Here, the institute is responsible for the above-mentioned fields within the curricula of „Geodesy and Geoinformatics“ (Master and Bachelor courses of study) as well as for „GEOENGINE“ (Master for Geomatics Engineering in English). In addition, the IIGS provides several courses in German for the curricula of „Aerospace Engineering“ (Bachelor and Master), „Civil Engineering“ (Bachelor and Master), „Transport Engineering“ (Bachelor and Master) and „Technique and Economy of Real Estate“ (Bachelor). Furthermore, lectures are given in English to students within the master course „Infrastructure Planning“. Finally, eLearning modules are applied in different curricula.

The current research and project work of the institute is expressed in the course contents, thus always presenting the actual state-of-the-art to the students. As a benefit of this, student research projects and theses are often implemented in close cooperation with the industry and external research partners. The main research focuses on kinematic and static positioning, analysis of engineering surveying processes and construction processes, machine guidance, monitoring, transport and aviation telematics, process and quality modeling. The daily work is characterized by intensive co-operation with other engineering disciplines, especially with traffic engineering, civil engineering, architecture, and aerospace engineering.

Research and Development

Improving the Quality of Low-Cost GPS Receiver Data Using Temporal Correlations

The investigations on low-cost single frequency GPS receivers at the Institute of Engineering Geodesy (IIGS) show that u-blox LEA-6T GPS receivers combined with Trimble Bullet III GPS antennas containing self-constructed L1-optimized choke rings can already obtain an accuracy in the range of millimeters which meets the requirements of geodetic precise monitoring applications. However, the quality (accuracy and reliability) of low-cost GPS receiver data, particularly in shadowing environment, should still be improved, since the multipath effects are the major error for the short baselines. The multipath effect is changing continuously with the time, i.e. it is temporally correlated. The temporal correlation of the multipath effect is used to improve the quality of low-cost GPS receiver data.

The multipath effect is periodic and a so-called multipath frequency of the carrier-phase can be modelled, if the geometric relationship between satellites, antenna and reflectors is known exactly, normally this is unknown in practice. Many satellites and reflectors are in the vicinity of the antenna, so that the multipath effect of the position is a mixture of the effects of the different pseudo ranges. The other problem is that the multipath frequency is changing with time because of the satellites also changing their positions constantly.

The idea is to calculate the precise multipath frequencies $f_{\delta\varphi,j}$ (compare equation (1)) within a short time period and to reduce these periodic effects in the GPS time series.

$$x_i = \sum_{j=1}^{q} a_j \cdot \sin\left(2\pi \cdot f_{\delta\varphi,j} \cdot t_k\right) + b_j \cdot \cos\left(2\pi \cdot f_{\delta\varphi,j} \cdot t_k\right)$$

The precise multipath frequencies $f_{\delta\varphi,j}$ can be calculated in two steps:

- The value of the multipath frequencies $f_{\delta\varphi,j}$ will be estimated roughly from the periodogram (step1).
- Since the frequencies in the periodogram are discrete, the precise multipath frequencies $f_{\delta\varphi,j}$ will be estimated in the neighborhood of the found frequencies from the step 1 by adjustment. The frequencies $f_{\delta\varphi,j}$ will be calculated iteratively until there are no more significant harmonic oscillations which are caused by the multipath effect.

The accuracy (standard deviation) of the low-cost GPS measurement can be improved by approx. 50% using this method.

Positioning of a Survey Vessel: Improved System Model for an Filter Algorithm

The HydrOs system focuses on the supply of precise positions and orientations on inland waterways. For this purpose, an evaluation software including an Extended Kalman Filter (EKF) was implemented and the measurements of a multi-sensor system are used as input (l_k at epoch t_k). Such a multi-sensor system was installed on the survey vessel „Mercator“ of the WSA Duisburg.

An EKF algorithm consists of two computation steps: The prediction step which is expressed by the system model and the update step with an observation model.

To achieve further improvements of the resulting positions and orientation angles, the system model and consequently the filter algorithm is expanded as a dynamic system (with memory effect).

It is assumed that accelerations being caused by the vessel propulsion, current, and wind can be modeled if the proper regulating variables are captured. In these cases, a delayed reaction to effective changes in acting forces is observed. So, a term describing a time-delayed proportional response characteristic can be used to model current accelerations, especially in the horizontal velocity components.

Other acting forces (caused by waves, vessel engine, passing ships, etc.) are not included in this deterministic model. They influence especially the roll rate ω_x, the pitch rate ω_y as well as the vertical velocity v_z and the corresponding accelerations. By looking at the measurement details, it is obvious that they include oscillations. For the integration of these remaining, non-modeled accelerations, a geometric prediction is chosen. Therefore, the resulting oscillation characteristics must be investigated, especially the occurring frequencies. For this purpose, Short Time Fourier Transform (STFT) and Continuous Wavelet Transform (CWT) are applied. In the second case, a transfer into the frequency domain is implemented.

The results of the analyzed roll rates (see Figure 1) / roll accelerations are shown in Figure 2. Oscillations in the three parts (downstream - turn - upstream) vary with regard to their amplitudes and the occurring frequencies. Therefore, it is necessary to model oscillations locally. The local oscillation parameters are computed by using the Gauß-Markov model for observations at epochs (t_{k-n}, t_k). The estimated parameters at epoch t_k permit an approximation of the accelerations which are inserted into the the EKF. Hence, the prediction of the state variables $\bar{x}_{k+1}$ can be improved (see Figure 3), which is visible in reduced innovations d_{k+1},

$$d_{k+1} = l_{k+1} - a_{k+1}(\bar{x}_{k+1}),$$

where $a_{k+1}(\bar{x}_{k+1})$ are the observation equations.

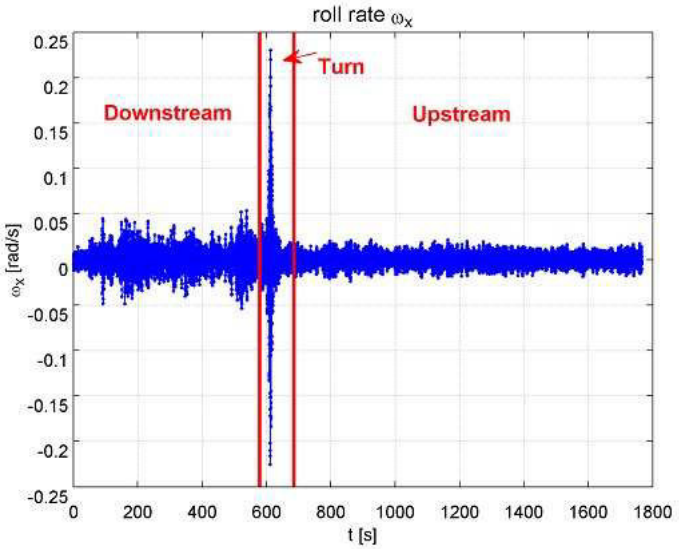

Figure 1: Measured roll rates

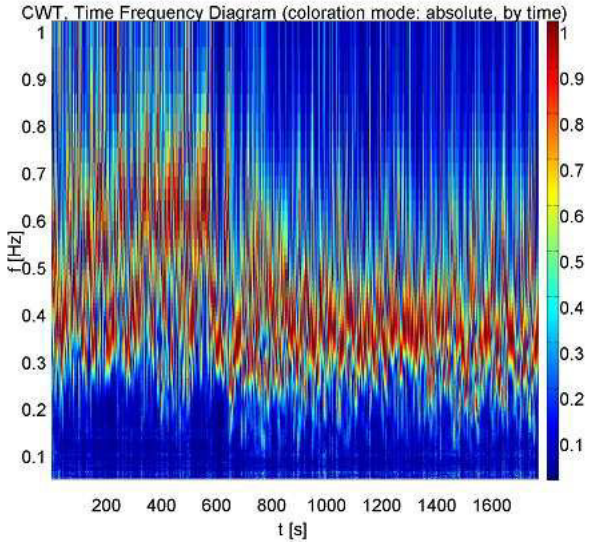

Figure 2: CWT Time Frequency diagram of $\delta\omega_x/\delta\Delta t$ (absolute values, coloration by time epoch)

The improvements can be expressed numerically by comparing the Root Mean Square (RMS) values of the innovations resulting from the previous prediction model with those of the extended dynamic system model. Table 1 shows the percentage reduction of these RMS values for the velocity components of the state vector.

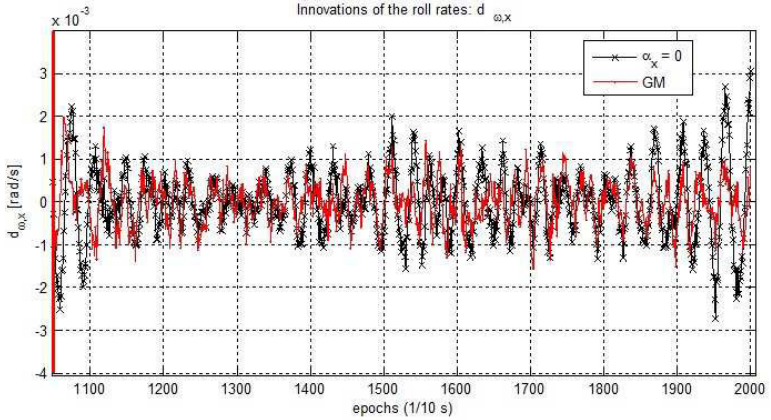

Figure 3: Innovations $d_{\omega,x,k}$ of the roll rates for a model without angular accelarations ($\alpha_x = 0$) and with approximated angular accelerations, which are computed by using the estimated oscillation parameters (GM). (Measurements of Kongsberg MRU5+)

Velocity component	ω_x	ω_y	ω_z	v_x	v_y	v_z
Improvement	53 %	42 %	5 %	35 %	13 %	14 %

Table1: Percentage reduction of the RMS values of the innovations for the filter approach with a dynamic system extension compared to the old model

Evaluation of the Control Quality for Tachymetric Controlled Vehicles

The control quality of a model truck in the scale 1:14, which is part of the construction machine simulator that has been developed at the Institute of Engineering Geodesy, University of Stuttgart, is investigated. The simulator system allows to test and evaluate the performance of different sensors or sensor combinations, as well as filter and control algorithms. In the present configuration, the simulator is able among others to perform lateral control of the model truck which moves automatically along a predefined reference trajectory. A robot tachymeter is the controlling sensor. For the evaluation, the laser tracker *API Radian* is used in combination with an active target as an external measurement system (s. Figure 4 and Figure 5).

Figure 4: Laser Tracker API Radian and Active Target (Automated Precision Inc., 2014)

The IIGS simulator system comprises a control computer, a robot tachymeter Leica TCRP1201 in combination with a 360° prism GRZ101, an A/D converter, a remote control and the mentioned model truck. The control of the model truck is realized by a closed-loop-system. The loop performs as follows: the tachymeter measures the position of the prism $y(t)$, mounted on the truck at the center of gravity and sends it to the control computer. The computer calculates the perpendicular distance / lateral deviation $e(t)$ between the truck position and the reference trajectory. Based on this information, the algorithm calculates the best steering angle $u(t)$ to guide the truck back on the reference trajectory as fast as possible. This sequence is executed 8 to 10 times per second. This rate is mainly depending on the kinematic measurement ability of the used robot tachymeter.

The distance measurement accuracy of the used laser tracker is 250 times better than that of the tachymeter. The angle measurement accuracy for both devices is at the same level. The active target has the ability to permanently align with the tracker's laser beam and thus always keep the line of sight, independently of the platform orientation. The use of this accurate external device allows to separate the control quality and the measurement accuracy from the resulting perpendicular distance, respectively lateral deviation $e(t)$. In consideration of the fact that $e(t)$ consists of the two quantities to be separated, we can define this value as combined measure.

The minimization of $e(t)$ within the system is carried out by a PID controller. The control quality of a given controlled system mainly depends on the choice of the controllers and is described as the remaining control deviation. Hypothetically, this value must reach zero. One definition of control quality is the root mean square (RMS), stated as follows:

$$RMS = \sqrt{\frac{\sum_{i=1}^{n} {e_i}^2}{n}}, \qquad (2)$$

e - lateral deviation, n - number of measurements.

Figure 5: Target Device Combination: Active Target and 360° Prism GRZ101

The quality parameters can be derived from the consideration of the differences between the reference trajectory, the recorded tachymeter trajectory and the recorded laser tracker trajectory. Thus, the following specifications for quality parameters can be defined: the RMS between the reference trajectory and the recorded tachymeter trajectory is defined as combined measure, containing the control quality and the measurement accuracy. The RMS between the reference trajectory and the recorded laser tracker trajectory represents the control quality and the RMS between the tachymeter and the laser tracker trajectory represents the measurement accuracy.

In the test scenario, two different trajectories in the shape of an „oval“ and an „eight“ were driven. Both trajectories contain the route design elements, like clothoides, circle arcs and straights. A PID controller, with empirically determined parameters, has been used. The data acquisition mode of the laser tracker was set to temporal discretization with a rate of 10 Hertz. The tracker was run simultaneously to the closed-loop of the tachymeter and vehicle operations. Table 2 depicts the achieved results.

	Combined Measure [m]	Control Quality [m]	Measurement Accuracy [m]
“Oval”	*0.0029*	*0.0031*	*0.0028*
“Eight”	*0.0028*	*0.0031*	*0.0029*

Table 2: Resulting RMS for the Quality Parameters

Reconsidering the definition for quality parameters, where the combined measure partly consists of the control quality and the measurement accuracy, it can be expected that the quadratic sum of these two RMS values must result in the RMS of the combined measure. Obviously, that is not the case. The consequential assumption is that unknown systematic effects affect the measurements. These effects could not be revealed yet, only by observing the combined measure. For the first time, this procedure of separating control quality and measurement accuracy allows to detect such effects, which is one of the benefits of the presented laser-tracker based evaluation system.

Impact of Terrestrial Laser Scanning Error Sources

This work is part of the project IMKAD, which is funded by the Deutsche Forschungsgemeinschaft (DFG) and realized in cooperation between the Institute of Engineering Geodesy, University of Stuttgart, and the Department of Geodesy and Geoinformation, Vienna University of Technology.

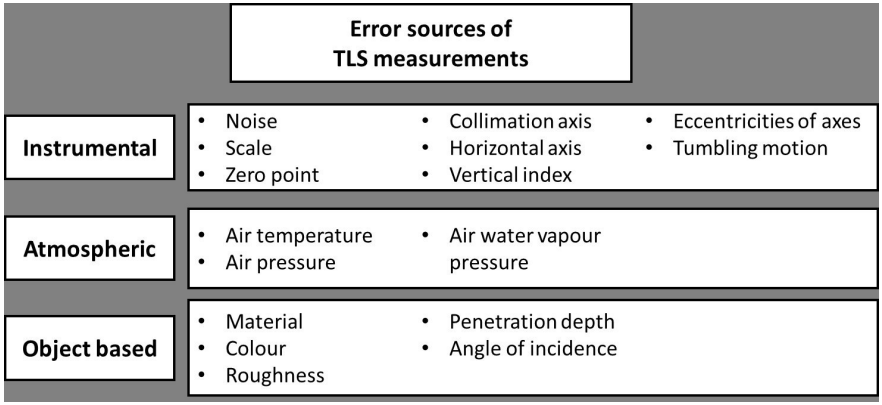

Figure 6: Error sources of terrestrial laser scanning measurements

A synthetic covariance matrix allows to investigate correlations within a point cloud. This matrix contains variances and co-variances based on the functional models of the main influences on measurements, e.g. a terrestrial laser scanning (TLS) point cloud. Figure 6 presents the error sources and their grouping into the three main parts for laser scanning measurements: instrumental errors, atmospheric errors and object-based errors.

In order to compute the correlations, these error sources must be classified into non-correlating, functional correlating, and stochastic correlating groups. The latest is the most challenging part, since the errors show complex relations between surface characteristics and incidence angles. Since the functional relation of these impacts cannot be separated completely, their correlations are computed by assuming an exponential curve as correlation function. For simulation, different data sets are generated, e.g. a grid with the size of 30 cm x 25 cm at 5 m distance (dataset 1) and a grid with the size of 65 m x 55 m at 50 m distance (dataset 2).

By determining the synthetic covariance matrix to dataset 1 and dataset 2, the impact of each error source can be evaluated. In figure 7, dataset 1 is presented. In this case, 60% of the impacts on the three-dimensional positional error are caused by the instrumental error sources which affect the range measurements substantially. The mean error of position is up to 0.6 mm. With respect to the spatial correlations, the biggest impact is up to 90% which is caused by functional correlated range errors. In case of dataset 2, shown in figure 8, the three-dimensional positional error is affected essentially by the impact of the object-based errors due to bigger incidence angles. This group of errors also causes the main impact on the spatial correlations which is up to 95%.

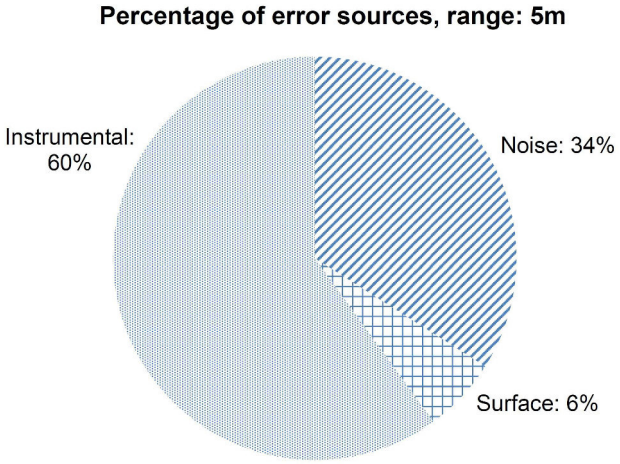

Figure 7: Percentage impact on 3D positional error, dataset 1; mean 3D positional error: 0.6 mm

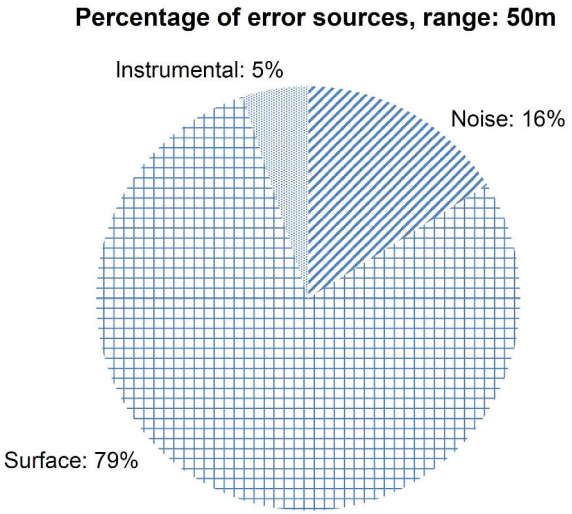

Figure 8: Percentage impact on 3D positional error, dataset 2; mean 3D positional error: 19 mm

As result, a synthetic covariance matrix might be considered for terrestrial laser scanning in order to take into account essential impacts. For future work, the investigations will focus on computing general correlation functions which might be valid for several datasets.

Geodetic Control of FEM-Model from Plane Load-Bearing Structures

Stuttgart Smartshell is a double-curved plane load-bearing structure with a base area of about 100 m^2 and a thickness of 4 cm, made of multilayer wood. Stuttgart SmartShell is resting on four supports. One of these supports is static, while the other three are mobile. The main reason to develop a structure like Stuttgart SmartShell is to investigate possibilities for constructions which offer an active manipulation in order to reduce structural vibrations and stress. In the same time the weight of the structure is reduced drastically. Figure 9 shows Stuttgart SmartShell.

Figure 9: Stuttgart SmartShell (©Bosch Rexroth)

The mobile supports of Stuttgart SmartShell could be moved in the three directions X, Y and Z. For the investigation with the Laser Scanner Leica HDS 7000, all supports are moved sequentially, in all three directions. After each measurement the support is moved back to the initial position. The movement is 20 mm in each direction.

The comparisons between the initial position and the different movements show results as expected by comparison to the FEM-Models. More interesting is the comparison between the FEM-Model and the scans in each position, because the scans show the actual measured state and the simulation shows the model state. For this comparison, the scans are transformed with a classical 3D-Helmert-Transformation to the coordinate system of the FEM-Model. The transformation parameters are determined once in the initial position and used for all other positions, too. Multiple statistical tests are made for all positions. Due to this test, there are no significant deviations, but the results are not realistic, because the deviations of more than 33 mm occur. One reason for the fact that these deviations are non-significant may be the correlations between the measurements.

In another step, laserscanning data from 2012 was compared with the current data set of the initial position. The two data sets were transformed as well and compared. This comparison shows significant deviations at one support. Reasons for those deviations could be the ageing of the

structure and the influence of the weather. These deviations led to a fracture of the structure. After fixing the structure, a new CAD model was created from laserscanning data.

The next steps should be the integration of influences due to weather, waterproofing and grinding into the FEM-Model. For further scans, the scanner errors should be investigated in detail and considered in the tests.

Ghosthunter - Telematics System Against Ghost Drivers Using GNSS

After the data quality evaluation of four different digital road maps (HERE, TomTom, OpenStreetMap and ATKIS-Basis-DLM) had been conducted, a weighting-function based map-matching algorithm was developed and implemented within the research project Ghosthunter that is cooperation with the University of the Armed Forces Munich (UniBwM) and the company NavCert in Brunswick. A map-matching algorithm is utilized to localize and to allocate the measured vehicle position based on GNSS signals on the most probable road link in a given digital road network database. In the preliminary studies, various criteria in terms of similarity between the vehicle trajectory and the matched digital road link are employed for an unambiguous correct identification of the correct road link on which the vehicle is travelling. As similarity criteria, heading, proximity (closeness) and link connectivity are chosen in this work.

The heading criterion describes the difference between the heading angles of the vehicle and a certain road link, which can be expressed as a cosine function (see Equation (1)). Thus, the less the $\Delta\alpha$, the higher the weight $f(\Delta\alpha)$ will be:

$$f(\Delta\alpha) = \cos(\Delta\alpha), \tag{3}$$

where the difference $\Delta\alpha$ between these two headings is defined as the angle between two 2D vectors, the directional vectors v_1 and v_2 respectively:

$$\Delta\alpha = \begin{cases} \arccos\left(\dfrac{\mathbf{v}_1 \cdot \mathbf{v}_2}{|\mathbf{v}_1| \cdot |\mathbf{v}_2|}\right), & 0° \le \Delta\alpha \le 90°; \\ 180° - \arccos\left(\dfrac{\mathbf{v}_1 \cdot \mathbf{v}_2}{|\mathbf{v}_1| \cdot |\mathbf{v}_2|}\right), & 90° < \Delta\alpha \le 180°. \end{cases} \tag{4}$$

Besides the heading criterion, the proximity criterion depending on the distance from a point to a line in 2D, which is calculated as follows:

$$D = \frac{x_3(y_1 - y_2) - y_3(x_1 - x_2) + x_3(x_1 y_2 - x_2 y_1)}{\sqrt{(x_1 - x_2)^2 + (y_1 - y_2)^2}} \tag{5}$$

where (x_3, y_3) are the coordinates of a measured vehicle position, the points (x_1, y_1) and (x_2, y_2) are the start point and the endpoint of a road link, respectively.

The last criterion considered in the proposed algorithm is the link connectivity that is denoted as,

$$X = \begin{cases} 1 & \text{with connectivity;} \\ 0 & \text{without connectivity.} \end{cases} \tag{6}$$

Using the above introduced similarity criteria, the corresponding weighting-function is expressed as:

$$TWS_i = \begin{cases} H_w \cos(\Delta\alpha) + D_w \left(\dfrac{\sqrt{2}b - D}{\sqrt{2}b} \right), & i = 2; \\ H_w \cos(\Delta\alpha) + D_w \left(\dfrac{\sqrt{2}b - D}{\sqrt{2}b} \right) + C_w X, & i \geq 3; \end{cases} \tag{7}$$

where the total weighting score (TWS) for the i-th measured vehicle position is determined from the weight coefficients H_w, D_w and C_w as well as the parameters $\Delta\alpha$, D and X related to heading, proximity and link connectivity criterion in Equation (2), (3) and (4); the variable b is used to define the buffer size. As the second point of the vehicle trajectory has no previous matched road link, the coefficient C_w is set to be zero for i = 2. Additionally, it is suitable for H_w, D_w and C_w to take the values in the following equations:

$$\begin{aligned} H_w &= 0.5,\ D_w = 0.5, && i = 2, \\ H_w &= \frac{1}{3},\ D_w = \frac{1}{3},\ C_w = \frac{1}{3}, && i \geq 3. \end{aligned} \tag{8}$$

For testing the correctness of the proposed map-matching algorithm, 35 real-world trajectories datasets and 37 simulated ones were generated und utilized. As illustrated in the figures below, the vehicle positions are completely correctly (100%) matched to the corresponding road segments. It can be demonstrated quite satisfactorily that the developed map-matching algorithm in this work is capable to provide highly correct map-matching results. For each vehicle position, the maximum time consumed by the map-matching process is less than 100 milliseconds. Thus, this map-matching algorithm has been found to be accurate and efficient to locate the vehicle position in the digital road map data, and it is very promising to be applied for the proposed wrong-way driving detection.

This work results from the research project Ghosthunter, which has been granted and funded by the German Federal Ministry for Economic Affairs and Energy (BMWi) and the German Aerospace Centre (DLR) under grant number 50 NA 1524.

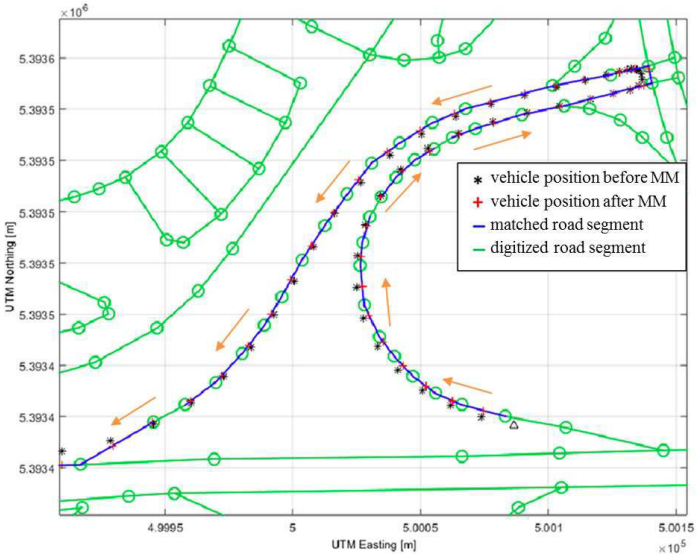

Figure 10: Map-matching results using GNSS-based real-world trajectory data

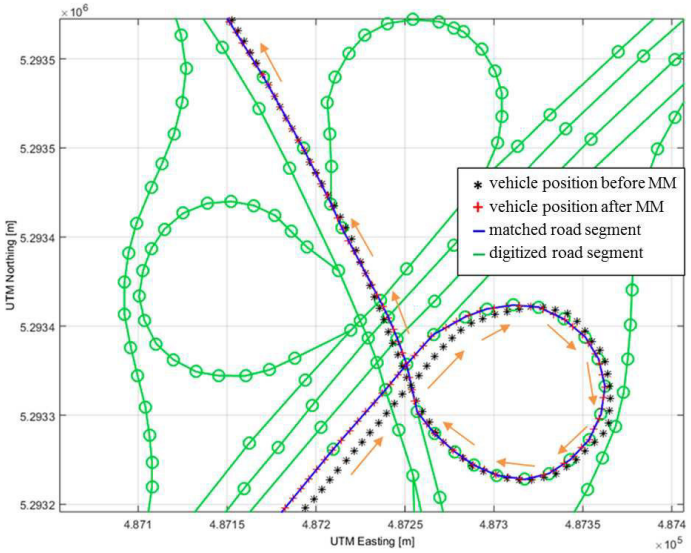

Figure 11: Map-matching results using simulated trajectory data

Publications

Refereed Publications

Abdallah, A., Schwieger, V.: Static GNSS Precise Point Positioning Using Free Online Services for Africa. Journal of Survey Review, 47 (346), pp. 61-77, Taylor & Francis, Bristol, United Kingdom.

Harmening, C., Kauker, S., Neuner, H., Schwieger, V.: Terrestrial Laserscanning - Modeling of Correlations and Surface Deformations. FIG Working Week 2016, 02-06.05.2016, Christchurch, New Zealand.

Kauker, S., Holst, Ch., Schwieger, V., Kuhlmann, H., Schön, S.: Spatio-Temporal Correlations of Terrestrial Laser Scanning. Allgemeine Vermessungsnachrichten, 6/2016, S. 170-182, Wichmann Verlag im VDE VERLAG GMBH, Berlin.

Kauker, S., Schwieger, V.: First Investigations for a Synthetic Covariance Matrix for Monitoring by Terrestrial Laser Scanning. In: 3rd Joint International Symposium on Deformation Monitoring (JISDM), 30.03-01.04.2016, Vienna, Austria.

Poptean, S., Jocea, A., Schmitt, A., Schwieger, V., Heidingsfeld, M., Sawodny, O.: Applications of Terrestrial Laser Scanning for Deformation Analyses of an Adaptive Supporting Structure. In: 3rd Joint International Symposium on Deformation Monitoring (JISDM), 30.03-01.04.2016, Vienna, Austria.

Wujanz, D.; Holst, C.; Neitzel, F.; Kuhlmann, H.; Niemeier, W.; Schwieger,V.: Survey Configuration for Terrestrial Laser Scanning. Allgemeine Vermessungsnachrichten, 6/2016, S. 158-169, Wichmann Verlag im VDE VERLAG GMBH, Berlin.

Zhang, L.; Schwieger, V.: Improving the Quality of Low-Cost GPS Receiver Data for Monitoring Using Spatial Correlations. In: Journal of Applied Geodesy 2016, 10(2): pp 119-129, De Gruyter, Germany.

Zhang, L.; Schwieger, V.: Improving the Quality of Low-Cost GPS Receiver Data for Monitoring Using Spatial Correlations. In: 3rd Joint International Symposium on Deformation Monitoring (JISDM), 30.03-01.04.2016, Vienna, Austria.

Non-Refereed Publications

Abdallah, A.; Schwieger, V.: Performance of IGS Final Satellite Data for Kinematic PPP Solutions Using Bernese Solutions and CSRS-PPP Online Service. GeoSiberia 2016, 20.-22.04.2016, Novosibirsk, Russia

Al-Mistarehi, B.; Schwieger, V.: Automatic Classification for Pavement Cracks for Mobile Mapping Data. FIG Working Week 2016, 02-06.05.2016, Christchurch, New Zealand.

Artz, T., Scheider, A., Breitenfeld, M., Brüggemann, T., Schwieger, V., Wirth, H.: Improved Positioning of Surveying Vessels on Inland Waterways with HydrOs. Hydrographische Nachrichten (HN 105), 11/2016, S. 34 - 38; und HYDRO 2016, Rostock-Warnemünde, 08.-10.11.2016

Frankl, K., Beckmann, H., Wang, J., Metzner, M., Schwieger, V., Eissfeller, B.: Preconditions for a Reliable & Robust Detection of Wrong-Way Driving on Highways with GNSS and Autonomous Sensors. 29th International Technical Meeting of the Satellite Division of The Institute of Navigation ION GNSS+ 2016, 12.-16.09.2016, Oregon Convention Center, USA.

Scheider, A.; Hassan, A.; Schwieger, V.; Breitenfeld, M.; Brüggemann, T.: Erweiterte Echtzeit- und Postprocessing-Verfahren zur Optimierung der GNSS-Ortung in Abschattungsbereichen an BWaStr. (Projektabschlussbericht HydrOs II) BfG-Bericht BfG-1892

Wang, J., Metzner, M., Schwieger, V.: Überprüfung und Bewertung der Datenqualität von digitalen Straßenkarten - Kartenvergleich zwischen HERE, TomTom, OSM und ATKIS-Basis-DLM, DGON-Symposium POSNAV, Berlin.

Presentations

Lerke, O., Schwieger V.: Evaluation of the Control Quality for Tachymetric Controlled Vehicles; MCG 2016 - 5th International Conference on Machine Control & Guidance, 5./6.10.2016; Vichy, France.

Pham, D.; Schwieger, V.: Comparison of filtering algorithms in vehicle positioning by using low-cost sensors. MCG 2016 - 5th International Conference on Machine Control & Guidance, 5./6.10.2016; Vichy, France.

Schwieger, V.: Low-Cost GPS for Monitoring - Improvement by Using Spatial Correlations. 16.05.2016, Chinese Academy of Surveying and Mapping; 18.05.2016, Wuhan University; 20.05.2016, Tongji University, China.

Schwieger, V.: Introduction on Faculty of Aerospace Engineering and Geodesy as well as Institute of Engineering Geodesy. 16.05.2016, Chinese Academy of Surveying and Mapping; 18.05.2016, Wuhan University; 20.05.2016, Tongji University, China.

Schwieger, V.: First Investigations for a Synthetic Covariance Matrix for Monitoring by Terrestrial Laser Scanning. First Workshop of DAAD Thematic Network „Modern Geodetic Space Techniques for Global Change Monitoring“, 20.-22.07.2016, Stuttgart, Germany.

Schwieger, V.: Qualitätssicherung in der Ingenieurgeodäsie - ein Überblick. 153. DVW Seminar Qualitätssicherung geodätischer Mess- und Auswerteverfahren, 23./24.06.2016, Hannover, Germany.

Schwieger, V.: Construction Machine Guidance. 31.10.-02.11.2016, Technical University of Construction Bucharest, Romania.

Schwieger, V.: Low Cost GNSS. 31.10.-02.11.2016, Technical University of Construction Bucharest, Romania,

Schwieger, V.: Terrestrial Laser Scanning. 31.10.-02.11.2016, Technical University of Construction Bucharest, Romania.

Schwieger, V.: Map Matching Applications. 24.11.2016, Seminar SE 3.05 „GPS/INS-Integration und Multisensor-Navigation“, Carl-Cranz-Gesellschaft e.V., Oberpfaffenhofen.

Activities at the University and in National and International Organisations

Volker Schwieger
- Dean of Faculty of Aerospace Engineering and Geodesy, University of Stuttgart
- Chair of FIG Commission 5 „Positioning and Measurement“
- Head of Working Group III „Measurement Methods and Systems“ of Deutscher Verein für Vermessungswesen (DVW)
- Chief Editor of Peer Review Processes for FIG Working Weeks and Congresses
- Member of Editorial Board Journal of Applied Geodesy
- Member of Editorial Board Journal of Applied Engineering Science
- Member of Editorial Board Journal of Geodesy and Geoinformation

Martin Metzner
- Member of the NA 005-03-01 AA „Geodäsie“ at the DIN German Institute for Standardization

Li Zhang
- Vicechair of Administration of FIG Commission 5 „Positioning and Measurement“
- Member of Working Group III „Measurement Methods and Systems“ of Deutscher Verein für Vermessungswesen (DVW)

Doctorates

Abdallah, Ashraf Talaat Mohammad: Precise point positioning for kinematic applications to improve hydrographic survey. Hauptberichter: Prof. Dr.-Ing. habil. V. Schwieger, Mitberichter: Prof. Dr. sc.-techn. W. Keller. Online Publikationen der Universität Stuttgart http://dx.doi.org/10.18419/opus-9026

Schützle, Rainer: Entwicklung und Evaluierung eines formgestützten Location Referencing Verfahrens München 2016, ISBN 978-3-7696-5193-5, Hauptberichter: Prof. Dr.-Ing. habil. V. Schwieger, Mitberichter: Prof. Dr.-Ing. L. Meng, Prof. Dr.-Ing. D. Fritsch. Online Publikationen der Universität Stuttgart: http://dx.doi.org/10.18419/opus-8971 und Bayerische Akademie der Wissenschaften, Verlag C. H. Beck, DGK, Reihe C, Nr. 776

Zhang, Li: Qualitätssteigerung von Low-Cost-GPS Zeitreihen für Monitoring Applikationen durch zeitlich-räumliche Korrelationsanalyse München 2016, ISBN 978-3-7696-5188-1, 170 S., Hauptberichter: Prof. Dr.-Ing. habil. V. Schwieger, Mitberichter: Prof. Dr.-Ing. O. Heunecke, Prof. Dr.-Ing. habil. L. Wanninger. Online Publikationen der Universität Stuttgart: http://dx.doi.org/10.18419/opus-8940 und Bayerische Akademie der Wissenschaften, Verlag C. H. Beck, DGK, Reihe C, Nr. 781

Diploma Theses and Master Theses

Friedrich, Janina: Geodätische Aufnahme des Flughafens Friedrichshafen zur Zertifizierung

Piesch, Simon: Programmierung einer Android-App zum Einrichten einer Referenzstation

Prică, Iulia-Mihaela: Investigation of the deformations of a timber plates pavilion (in cooperation with Technical University of Construction Bucharest)

Schirmer, Isabella: Geodätische Aufnahme des Flughafens Friedrichshafen zur Zertifizierung

Trusca, Sandra: Optimization of 2D and 3D Geodetic Networks (in cooperation with Technical University of Construction Bucharest)

Wenk, Maximilian: Untersuchung verschiedener Ansätze zur kinematischen Georeferenzierung für terrestrische Laserscanner

Zhang, Lifan: Accurate Geo-Referencing for Deformation Analysis by TLS

Study Theses and Bachelor Theses

Kohler, Stefan: Untersuchung einer optimalen Aufnahmekonfiguration für Laserscanner

Kokenbrink, Jana: Erstellung eines 3D CAD-Modells der Stuttgarter Smartshell durch Vermessung der Ist-Geometrie (In Zusammenarbeit mit dem Institut für Leichtbau Entwerfen und Konstruieren - ILEK)

Mayer, Lucas: Bewertung und Analyse der innerörtlichen Flurneuordnung zur Beseitigung ungeregelter Verhältnisse und Reaktivierung von Ortskernen

Ren, Wenhao: Qualitätsvergleich von SmartNet- und SAPOS-Dienst

Education

SS16 and WS16/17 with Lecture/Exercise/Practical Work/Seminar

Bachelor Geodesy and Geoinformatics (German)

Basic Geodetic Field Work (Schmitt, Kanzler)	0/0/5 days/0
Engineering Geodesy in Construction Processes (Schwieger, Hassan)	3/1/0/0
Geodetic Measurement Techniques I (Metzner, Schmitt)	3/1/0/0
Geodetic Measurement Techniques II (Schmitt)	0/1/0/0
Integrated Field Work (Kauker, Metzner)	0/0/10 days/0
Methods of Measurements and Analysis in Engineering Geodesy (Schwieger, Hassan, Kauker)	2/2/0/0
Reorganisation of Rural Regions (Helfert)	1/0/0/0
Statistics and Error Theory (Schwieger, Wang)	2/2/0/0

Master Geodesy and Geoinformatics (German)

Causes of Construction Deformation (Metzner, Wang)	1/1/0/0
Deformation Analysis (Zhang)	1/1/0/0
Industrial Metrology (Schwieger, Schmitt)	1/1/0/0
Land Development (Eisenmann)	1/0/0/0
Monitoring Measurements (Schwieger, Wang)	1/1/0/0
Monitoring Project (Lerke)	0/0/2/0
Thematic Cartography (Zhang, Kauker)	1/1/0/0
Transport Telematics (Metzner, Scheider)	2/2/0/0

Master GeoEngine (English)

Integrated Field Work (Kauker, Metzner)	0/0/10 days/0
Kinematic Measurement Systems (Schwieger, Lerke)	2/2/0/0
Monitoring (Schwieger, Wang)	1/1/0/0
Thematic Cartography (Zhang, Kauker)	1/1/0/0
Transport Telematics (Metzner, Scheider)	2/1/0/0
Terrestrial Multisensor Systems (Zhang, Lerke)	2/1/0/0

Bachelor and Master Aerospace Engineering (German)

Statistics for Aerospace Engineers (Zhang, Hassan)	1/1/0/0

Master Aerospace Engineering (German)

Transport Telematics (Metzner, Scheider)	2/2/0/0

Bachelor Civil Engineering (German)

Geodesy in Civil Engineering (Metzner, Hassan)	2/2/0/0

Master Civil Engineering (German)

Geoinformation Systems (Metzner, Lerke)	2/1/0/0
Transport Telematics (Metzner, Scheider)	1/1/0/0

Bachelor Technique and Economy of Real Estate (German)

Acquisition and Management of Planning Data and Statistics (Metzner, Kanzler)	2/2/0/0

Bachelor Transport Engineering (German)

Statistics (Metzner, Kanzler)	0.5/0.5/0/0
Seminar Introduction in Transport Engineering (Schmitt)	0/0/0/1

Master Infrastructure Planning (English)

GIS-based Data Acquisition (Zhang, Schmitt)	1/1/0/0

Institute of Geodesy

Geschwister-Scholl-Str. 24D, D-70174 Stuttgart,
Tel.: +49 711 685 83390, Fax: +49 711 685 83285
gis@gis.uni-stuttgart.de or firstname.secondname@gis.uni-stuttgart.de
http://www.gis.uni-stuttgart.de

Head of Institute

Prof. Dr.-Ing. Nico Sneeuw

Emeritus

em. Prof. Dr.-Ing. habil. Dr.tech.h.c.mult. Dr.-Ing.E.h.mult. Erik W. Grafarend

Academic Staff

Dr.-Ing. Markus Antoni	Physical Geodesy, Satellite Geodesy
Prof. Dr. sc. techn. Wolfgang Keller	Physical Geodesy, GNSS
Dr.-Ing. Friedrich Krumm	Adjustment Theory, Mathematical Geodesy
Dipl.-Ing. Matthias Roth	Physical Geodesy, Satellite Geodesy
Dr.-Ing. Mohammad Tourian	Satellite Geodesy, Hydrology

Research Associates

M.Sc. Omid Elmi	Remote Sensing
Dr.-Ing. Siavash Iran Pour (until 10.03.)	Future Satellite Missions
M.Sc. Muhammad A. Javaid	Satellite Geodesy
M.Sc. Wei Liu	Satellite Geodesy
M.Sc. Shirzad Roohi	Altimetry, Hydrology
M.Sc. Saemian Peyman (since 1.10.)	Satellite Geodesy, Hydrology
M. Tech. Bramha Dutt Vishwakarma	Hydrology, Filter Methods
Dipl.-Ing. Elisabeth Woisetschläger (since 1.12.)	Satellite Geodesy, Hydrology, Altimetry
M.Sc. Jinwei Zhang	Satellite Geodesy, Hydrology

Administrative/Technical Staff

Dipl.-Ing. (FH) Thomas Götz	IT System, Controlling
Dipl.-Betriebsw. (FH) Wanda Herzog	Study Course Management
Dipl.-Ing. (FH) Ron Schlesinger	IT System, Technical Support
Anita Vollmer	Secretary

Guests

Dr. Baogui Ke, CASM Beijing, China, (24.11.15–21.02.2016)
Prof. Ilias Tziavos, , Aristotle University of Thessaloniki, Greece (1.2.–29.4.)
Prof. Peter Varga, Geodetic and Geophysical Research Institute, Sopron, Hungary (1.3.–31.5.)
Prof. Dr. Hanjiang Wen, CASM Beijing/China (1.7.–19.8.)
Assoc. Prof. Yi Lin, Tongji/China (1.7.–9.9.)
Prof. Dr. Weiping Jiang, Wuhan University, China (1.7.–19.8.)
Assoc. Prof. Taoyong Jin, Wuhan University, China (1.7.–26.8.)
Prof. Zhengtao Wang, Wuhan University, China (1.7.–26.8.)
Prof. Jiexian Wang, Tongji University, China (1.8.–30.8.)
Prof. Lars Sjöberg, Royal Institute of Technology (KTH), Stockholm, Sweden (2.11.–30.11.)

Guests of DAAD Thematic Network

MSc Huanling Liu, Beijing, CASM, China, 24.11.15–21.2.16
MSc Xin Chang, Wuhan University, Wuhan, China, 1.11.15–15.11.16
MSc Bin Wang, Wuhan University, Wuhan, China, 1.11.15–15.11.16
MSc Junping Zou, Tongji University, Tongji, China, 23.11.15–18.2.16
MSc Jie Yu, Tongji University, Tongji, China, 23.11.15–18.2.16
PhD Peng Yuan, Wuhan University, Wuhan, China, 1.9.16–28.2.17
MSc Fei Yang, Tongji University, Tongji, China, 1.9.16–28.2.17
MSc Zhanglin Ye, Tongji University, Tongji, China, 1.9.16–30.11.16
PhD Weiwei Wu, Tongji University, Tongji, China, 1.12.16–28.2.17

External Lecturers

Dipl.-Ing. Steffen Bolenz, Stadtmessungsamt, Stuttgart
PD Dr.-Ing. habil. Johannes Engels, Stuttgart
Dipl.-Ing. Dieter Heß, Ministerium für Ländlichen Raum und Verbraucherschutz Baden-Württemberg, Stuttgart
Dipl.-Ing. Günther Steudle, Ministerium für Ländlichen Raum und Verbraucherschutz Baden-Württemberg, Stuttgart

Research

HydroSat: a Repository of Global Water Cycle Products from Spaceborne Geodetic Sensors

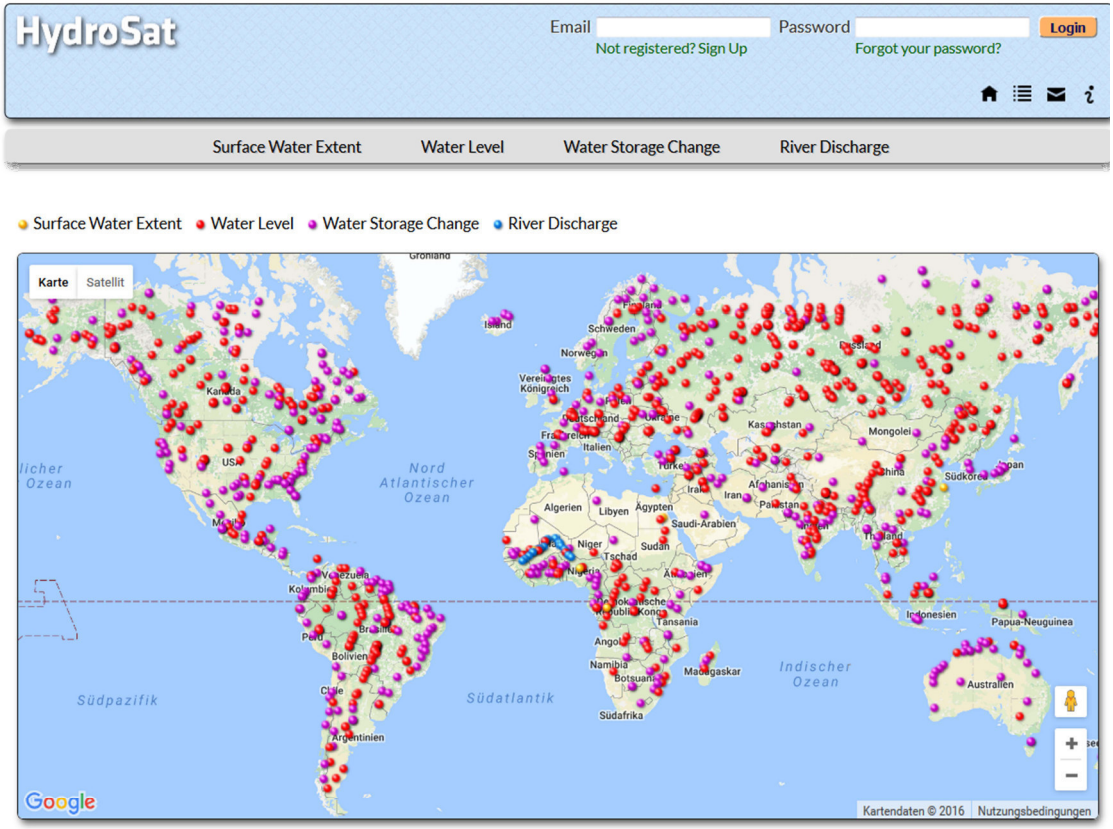

Figure 1: HydroSat website with global water cycle products from spaceborne geodetic sensors.

Against the backdrop of global change, both in terms of climate and demography, there is an increasing need for monitoring the global water cycle. The publicly available global database is very limited in its spatial and temporal coverage worldwide. Moreover, the acquisition of in situ data and their delivery to the database are on the decline since the late 1970s be it for economical, political or other reasons. Given the insufficient monitoring from in situ gauge networks, and

without any outlook of improvement, spaceborne approaches are currently being investigated. Satellite-based Earth observations with their global coverage and homogeneous accuracy have been demonstrated to be a potential alternative to in situ measurements. The Institute of Geodesy at University of Stuttgart (GIS) has a long-standing expertise, both theoretically and practically, in dynamic satellite geodesy. In recent years, GIS initiated and participated in studies and projects on the application of spaceborne geodetic sensors for hydrological studies. The results of these studies and projects are now available at HydroSat website http://hydrosat.gis.uni-stuttgart.de, which is freely accessible since November 2016.

HydroSat aims to provide information on continental waters using spaceborne geodetic sensors. The website provides

- ▷ Surface water extent of inland water bodies from satellite imagery
- ▷ Water level time series of inland water bodies from satellite altimetry
- ▷ Continental water storage changes from satellite gravimetry
- ▷ River discharge from satellite altimetry, imagery or gravimetry

River Discharge Estimation at Daily Resolution from Satellite Altimetry over an Entire River Basin

The global publicly available discharge database has steadily been declining over the past few years, leading to a demand for independent sensors and algorithms. Recent studies show that altimetric water height over rivers can sensibly be used to deal with this growing lack of discharge. Previous studies estimated river discharge through a one-to-one functional relationship of discharge and altimetric water level time series, known as *rating curve*. This model is typically derived from a non-linear regression of discharge vs. water level at the crossing of altimetry groundtrack and river, the so-called *virtual station*, whenever synchronous time series exist.

However, as a general problem of all estimated altimetric water level and discharge, the time resolution at the virtual stations is, in fact, dictated by the repeat period of the satellite orbit. This leads to a typical 10 days (Topex/Poseidon and Jason-series) or 35 days (ERS-series and ENVISAT, SARAL/AltiKa) temporal resolution.

Here, we suggested a method which goes beyond the conventional one-to-one relationship. Here, we estimate daily river discharge using a multitude of altimetric time series from different satellite altimetry missions over Niger River including its two major tributaries (Figure 2). Altimetric time series at virtual stations both upstream and downstream of the Inner Niger Delta are taken into account. To this end, we implement a linear dynamic system to (1) provide a scheme for data assimilation of multiple altimetric discharge along a river; (2) estimate daily discharge; (3) deal with data outages, and (4) smooth the estimated discharge. Our linear dynamic system consists of a stochastic process model that benefits from the cyclostationary behavior of the discharge. This means that our process model explicitly benefits from the seasonal statistical properties

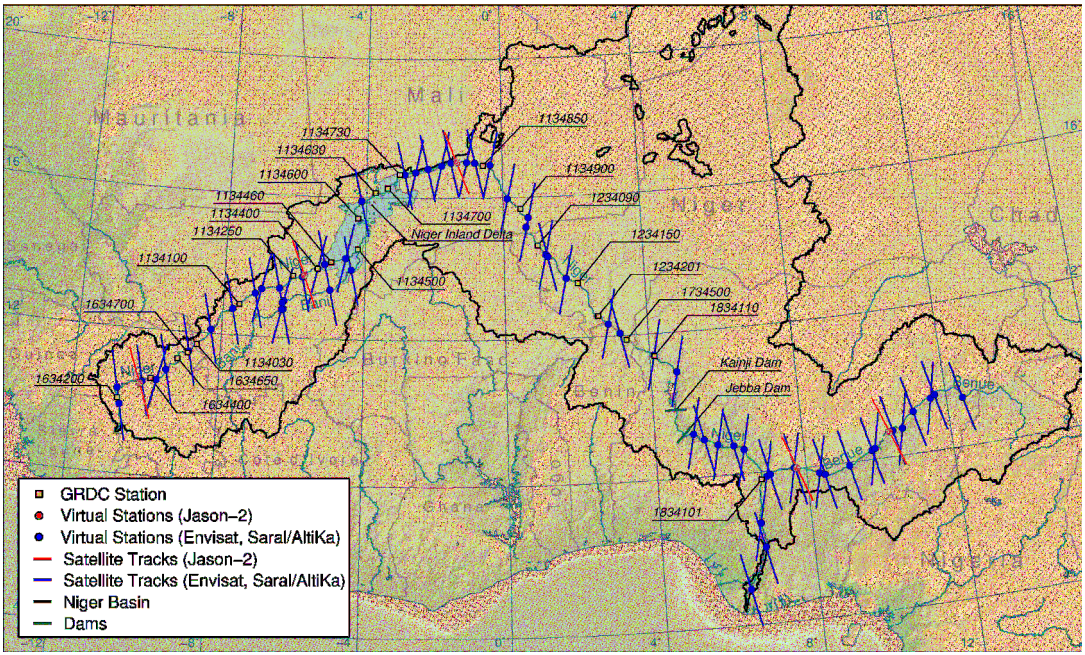

Figure 2: The Niger River flowing through 5 countries: Guinea, Mali, Niger, Benin, Nigeria and its two major tributaries Bani and Benue. Red and blue lines and dots represent the groundtrack and the selected virtual stations from Jason-2 and ENVISAT, SARAL/AltiKa, respectively.

of discharge. The process model comprises the covariance and cross-covariance information of river discharge along the river stream. The process model is combined with numerous altimetric discharge time series to form a linear dynamic system. We solve the linear dynamic system using the Kalman filter and smoother which provide unbiased discharge with minimum variance.

The unbiased solutions of the Kalman filter and smoother for the six observation equation variants were validated against *in situ* data at 18 gauges along the Niger River (Figure 3). Overall, our validation shows an average correlation of 0.9, an average relative RMSE and relative bias of 15%, $\mathrm{NSE}_{\mathrm{mean}}$ greater than 0.5 for 15 gauges and $\mathrm{NSE}_{\mathrm{cycle}}$ above 0 for all gauges.

Validation shows that our method can successfully estimate river discharge at daily resolution over an entire river basin. Our results for the previously gauged Niger basin are especially intriguing in light of the fact that many other river basins around the world suffer from the same poor discharge availability.

Developing such a method based on satellite altimetric data which provides a better estimation than the existing legacy mean daily discharge is highly beneficial for hydrological studies and

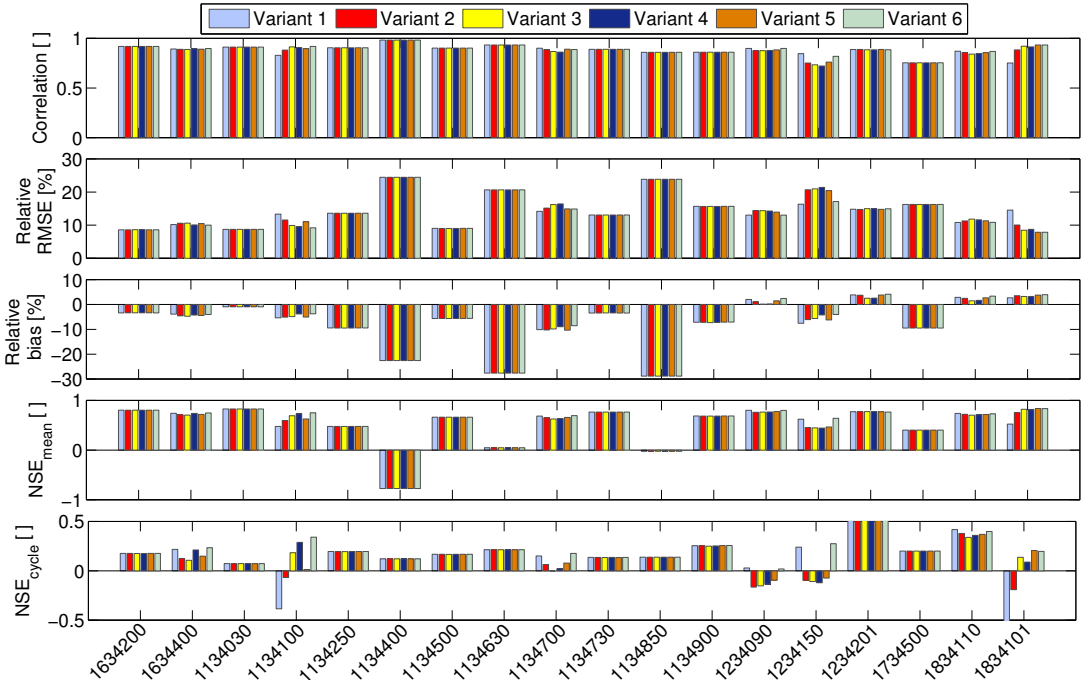

Figure 3: Performance metrics of estimated discharge time series at 18 gauging station along the Niger River for different variants of densification of altimetry.

hydraulic model calibration. Such benefit is more highlighted with the abundance of existing and future altimetry, including the operational Sentinel series of the European Copernicus program, but also including research satellites such as SARAL/AltiKa, Jason-3 or SWOT.

Dynamic River Masks from Multi-Temporal Satellite Imagery: An Automatic Algorithm Using Graph Cuts Optimization

Our knowledge of the spatio-temporal variation of river hydrological parameters is surprisingly poor. In situ gauge stations are limited in spatial and temporal coverage, and their number has been decreasing during the past decades. On the other hand, remote sensing techniques have proven their ability to measure different parameters within the Earth system. Satellite imagery, for instance, can provide variations in river area with appropriate temporal sampling. Water bodies appear very dark in the near-infrared (NIR) wavelength in optical images because Water absorbs nearly all sunlight in this domain. However, a precise recognition of water bodies is challenging in

some regions or seasons, because of the complex relationship between water and land in coastal areas, wet riparian zones, vegetated environments, and so on.

Thresholding an image to obtain the object is prevalent because of its efficiency and easy implementation. This technique is also widely used in inland water body monitoring to develop water masks. Apart from thresholding, other unsupervised and supervised classification algorithms are widely used to extract water bodies from satellite images. Under ideal conditions, dynamic thresholding techniques can extract water bodies precisely. However, various error sources and a complex relationship between water and land in coastal areas necessitate defining the threshold value in a supervised manner using visual inspection of the image histogram or manual trial-and-error procedures.

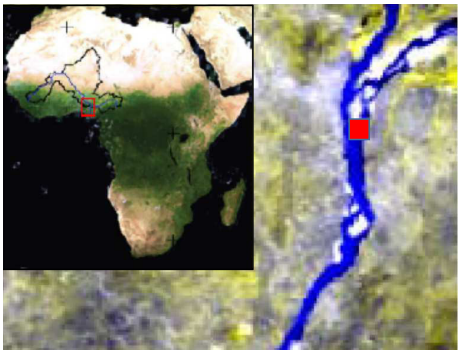

Figure 4: Part of Niger River selected as case study. The Lokaja location is defined by red box.

Beyond pixel intensity, the spatial correlation between neighboring pixels is a source of information that can be used to detect the changes among images. Like other natural phenomena, water bodies have a high spatial correlation in satellite images. So, including contextual information as an additional constraint in the procedure of water body monitoring should significantly improve the quality of final water masks. Moreover, every pixel has a particular temporal behavior, mainly driven by annual and seasonal climatology. So, in addition to spatial correlation, a strong temporal correlation is typically available. This feature is realized here using Markov Random Fields (MRF), which we can use to model the interaction between different constraints and auxiliary sources of information in an image. In image processing and remote sensing, developing an efficient MRF model and defining the maximum a posteriori (MAP) estimation under the model is a popular region-based classification approach.

We develop an automatic water body area monitoring algorithm for satellite images. In this algorithm, a MRF model was developed to consider pixel intensity and spatial and temporal interactions between pixels. Then, a maximum a MAP solution for the Bayesian framework was found to determine the most probable water mask. Since the high computational effort of finding a global solution is a serious concern, the problem was reshaped as an energy minimization.

$$E(f) = (1-\lambda)E_{\text{data}}(f) + \lambda E_{\text{smooth}}(f)$$

where $E_{\text{data}}(f)$ is a function that deals with the pixels value and their possible labels. $E_{\text{smooth}}(f)$ measures the agreement between adjacent pixels in terms of their value. $\lambda \in [0,1]$ is the balancing term allows us to control the contribution of each term to the total energy. To minimize the energy function, we have developed an undirected graph with two terminals and defined the max-flow

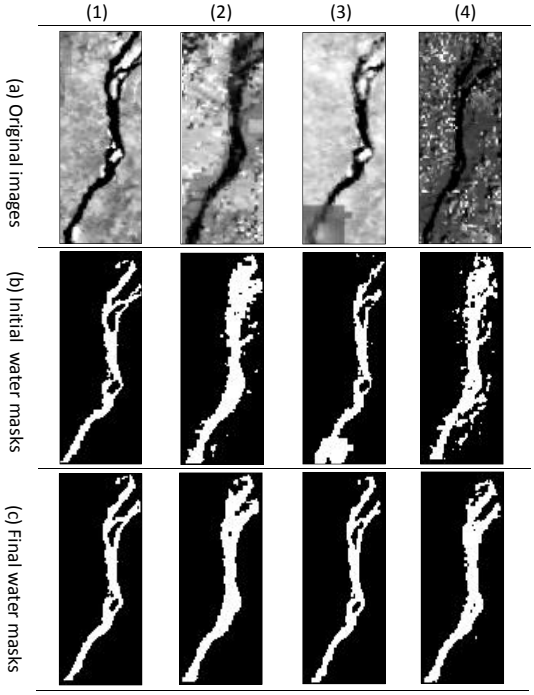

*Figure 5: Four examples of generated water masks in different situations. (**1**,**2**) relate to the dry and wet seasons. In (**3**,**4**), images suffer from cloud contamination.*

solution for the graph by augmenting all the possible paths between two terminals. The final residual graph offered the binary water mask representing the MAP solution. We apply it on MODIS images of the part of Niger River in Africa near Lokaja station (Figure 4)

To discuss the performance of the method, we compare four final water masks with the initial ones over the selected area (Figure 5). In Figure 5(a1) since the river borders are clearly distinctive in the initial water mask derived by k-means clustering (Figure 5(b1)), the accuracy improvement of river mask after applying the proposed method is not significant (Figure 5(c1)). In Figure 5(a2), we see that the adjacent areas of the river are also wet. As a consequence, the initial water mask (Figure 5(b2)) is not accurate, as some land pixels are labeled as water. However, the graph cuts method is able to overcome this situation to a large extent and improve the final water mask (Figure 5(c2)). Our algorithm is even able to remove most of the isolated pixels which are wrongly labeled as water in the initial water mask. In Figure 5(a3), the land around the river border in the bottom of the river is wet, and the upper part of the river is also covered by cloud. The graph cuts

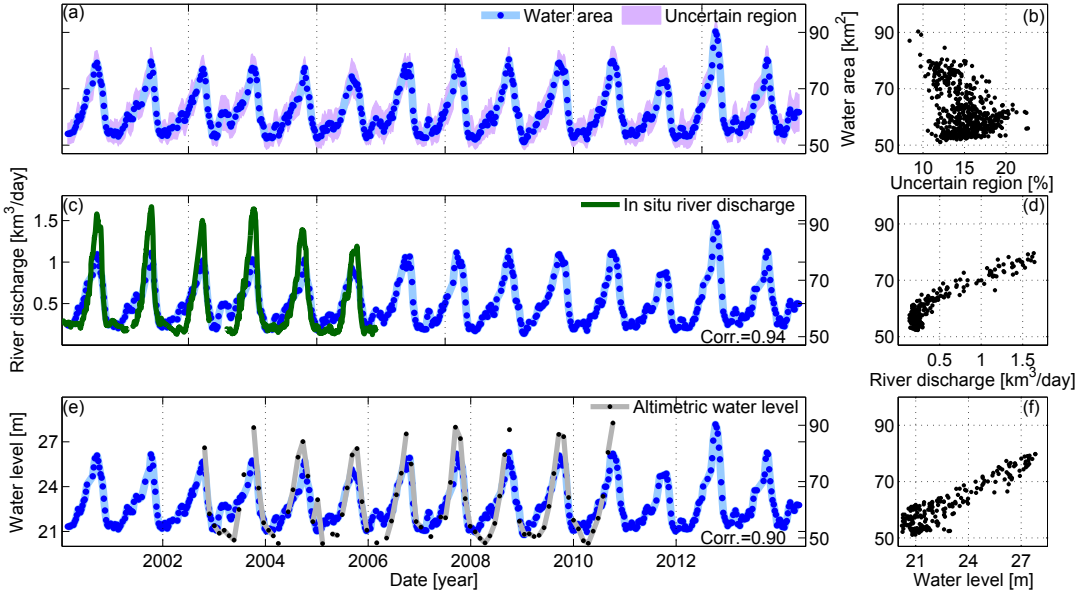

*Figure 6: (**a**) Water area with its uncertainty; (**b**) Scatter plot of water area vs. percentage uncertainty; (**c**,**d**) Water area is plotted with in situ discharge and altimetric water level, respectively; (**e**,**f**) Scatter plots of simultaneous water area measurements against discharge and water level, respectively. Period of monitoring: 02.2000–09.2014.*

method extracts the river from the surrounding wet area, and it can recover the cloudy part of the river (Figure 5(c3)). The last example reveals the ability of the method to ignore clouds and determine the water mask as accurately as possible (Figure 5(c4)). Such results indicate that the weight functions for defining graph edges are properly defined.

Our second aim is the uncertainty assessment of derived water masks. Therefore, we computed the confidence level for pixels by measuring the marginal probability of all nodes in the final residual graph. In order to generate a reliable water area time series, we accept the assigned labels for pixels with marginal probabilities higher than 10% in both water and land masks. This leaves a third region which contains pixels with marginal probabilities less than 10% in both masks. This is the uncertain region, for which we cannot define a proper label based on the available information. Figure 6(a) shows the result of our method for the selected area.

The blue dots in the time series represent the satellite observations. Figure 6(b) is a scatter plot of water area vs. uncertainty. It shows that the uncertainty varies between 9% and 22%, with average uncertainty being around 15% of the area.

In order to assess the correctness of our river area estimation, we compare with in situ river discharge and with altimetric water level measurements. In a natural river channel, there is a monotonic relationship between different river parameters like river discharge, width and hight. Therefore, the corresponding time series should show a significant correlation. The high correlation between the two time series (0.94) in Figure 6(c) indicates a high consistence between the behavior of water area and river discharge. The discharge–area scatter plot (Figure 6(d)) shows a non-linear relationship. Further, we compare water level with water area. To this end, we use water level from satellite altimetry, which overlaps with our water area estimation for the time period of 2002–2011 (Figure 6(e)). Similar to validation against discharge, the water level and water area are highly correlated (0.90). The scatter plot represents such high correlation between water area and height (Figure 6(f)).

Ocean Tide Aliasing in Spaceborne Gravimetry: a Data-driven Determination of the Tidal Alias Spectrum

Due to under-sampling from satellite orbit, high-frequency ocean tidal signals alias into the gravity signal. Likewise, errors in ocean tide models, used for de-aliasing in the gravity field retrieval, will directly alias into the recovered gravity field. Thus, ocean tides cause notable aliasing errors in the gravity field from single pair space-borne gravimetry missions like GRACE.

Several studies into future gravity missions have shown that constellations with two or more GRACE-like tandems lead to a significant reduction of aliasing error from all kinds of high-frequency signal sources. Despite such reduction, tidal aliasing will remain a residual error source. If the alias spectrum is known, the aliasing errors can be removed given a time series covering at least one cycle of the alias period. As the spectrum of ocean tide constituents is known precisely, the alias spectrum can be estimated in two ways: (1) analytical: formulating sampling behavior and estimating the alias frequencies together with the signal frequencies, (2) empirical: analyzing the only-tide-driven time series of simulated gravity fields and deriving the aliasing spectrum. Apart from the orbit sampling by certain satellites, the recovered gravity fields require signal averaging in time and in the spatial domain, which makes the sampling behavior more complicated than in the case of satellite altimetry.

Table 1: Main orbit parameters.

	β / α	I	altitude [km]
polar pair	172/11	92°	362
inclined pair	460/29	115°	342

Table 2: Simulation setup in two scenarios

scenario	formation type	constituents	time length
single pair	polar pair	M_2, N_2, S_2, K_2 O_1, P_1, Q_1, K_1	5 years
double pair	polar + inclined pair		

Here we investigate the alias characteristics of single pair and double pair formations by closed-loop simulation with individual ocean tide constituent and their combination. It should be reminded that no static gravity field and other temporal gravity signals are included as input except for the ocean tides. The difference of two tide models, GOT4.7 and EOT08a, is taken as the remain tidal errors to feed the simulation. Table 1 shows the main orbit setup and Table 2 refers to the scenarios for the simulation.

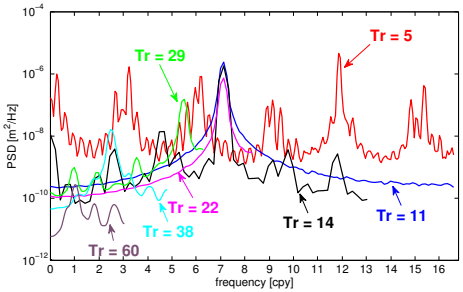

Figure 7: Alias spectrum of constituent M_2.

Figure 7 shows that different alias spectra show up with different recovery periods T_r for the constituent M_2. This demonstrates the complexity of the aliasing behavior induced by the spatial and temporal averaging during the gravity field retrieval. Without taking the retrieval procedure into consideration, the orbit sampling alone cannot give a comprehensive insight into tidal aliasing.

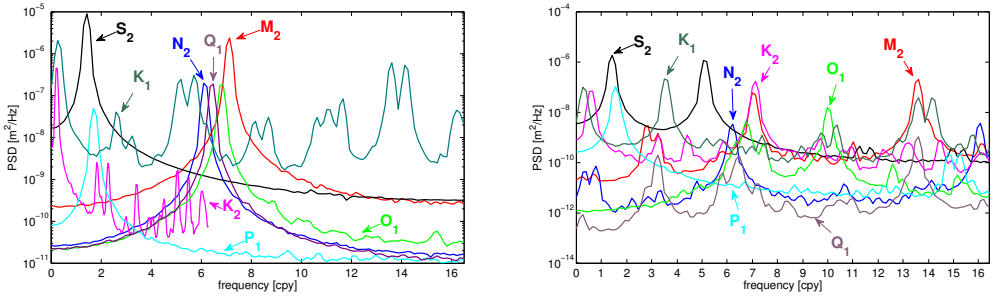

Figure 8: Alias spectra of 8 main tidal constituents for single pair (left) and double pair (right).

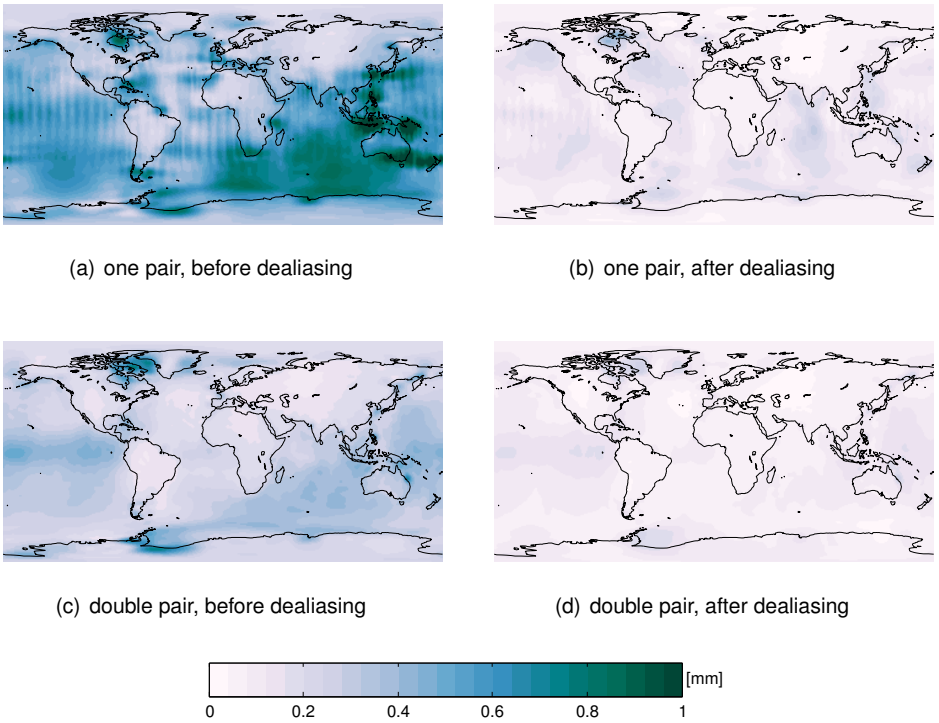

Figure 9: Alias error (in terms of geoid height rms) of single-pair and double-pair formation before de-aliasing for all constituents.

Figure 8 represents the aliasing periods of each constituent for one pair and double pair formations. The recovery period is the same as the repeat period of the polar pair. Based on the derived alias spectrum, the aliasing errors are calculated by least-squares estimation and removed from the gravity field time series. Figure 9 shows the geoid height rms before de-aliasing and after de-aliasing. As only ocean tide errors are included in the simulation, the before de-aliasing figures represent the aliasing error energy and the energy after de-aliasing is expected to be zero in an ideal situation. From Figure 9 we can conclude that the alias periods estimated by this data-driven method is good enough for applying to remove the aliasing errors. Moreover, a double-pair acts in a de-aliasing way in comparison to single-pair formation comparing two figures on the left.

Estimating the Leakage due to Filtering of GRACE Products

The noisy mass change estimates from GRACE are filtered to obtain useful information. Filtering suppresses noise but also changes the signal over a catchment by suppressing its amplitude and introducing leakage from nearby catchments. The leakage signal affects the amplitude and the phase of the catchment time series. Therefore, determining leakage and estimating its impact on the overall quality of the signal is vital for using GRACE in hydrology. However, computing leakage requires knowledge of the true field, which is unknown for GRACE, and a leakage from noisy fields is erroneous.

This is the reason many contributions prefer less accurate hydrological models for computing leakage. Such a practice propagates the error and uncertainties in models to the leakage. Therefore, we advocate using the filtered GRACE fields instead of models. Since filtering changes the information, the leakage from filtered fields is not the same as the true leakage. We found that the true leakage is stronger than the leakage from the once filtered field, and the leakage from the once filtered field is stronger than the leakage from the twice filtered fields. Furthermore, they are related by a similar amplitude ratio and phase change.

In order to estimate true leakage, we propose to first calculate the leakage time series from once filtered fields $\bar{l}_\mathrm{c}$ and leakage from twice filtered fields $\bar{\bar{l}}_\mathrm{c}$, then the phase difference between them. Shift the $\bar{\bar{l}}_\mathrm{c}$ by the phase difference towards $\bar{l}_\mathrm{c}$, and after removing outliers calculate the mean of the ratio between shifted $\bar{\bar{l}}_\mathrm{c}$ and $\bar{l}_\mathrm{c}$ at each time point. Then shift $\bar{l}_\mathrm{c}$ by the phase difference and multiply it by the mean ratio to get an estimate of the leakage $\hat{l}_\mathrm{c}$, which should be very close to the leakage time series l_c. Since the leakage is estimated from the data itself, it is called the data-driven approach.

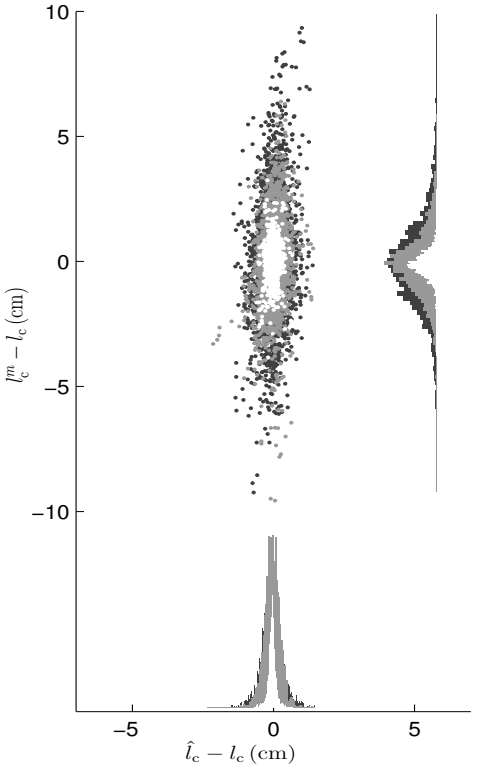

Figure 10: Histogram and scatter plot between the leakage error from a model and the leakage error from the data-driven approach. The three colours denote the three categories by catchment area: White $> 10^6\,\mathrm{km}^2$*,* $10^6\,\mathrm{km}^2 >$ *light gray* $> 250000\,\mathrm{km}^2$*, and dark gray* $< 250000\,\mathrm{km}^2$*.*

In Figure 10, we compare the leakage from WaterGap Hydrological Model (WGHM) fields with the data-driven leakage obtained from filtered Global Land Data Assimilation System (GLDAS) fields. The Figure shows a scatter plot of error in leakage along with their respective histograms for 127 catchments. The scatter plot is between the error in estimated leakage ($l_{\mathrm{c}} - \hat{l}_{\mathrm{c}}$), and the error in leakage from a model ($l_{\mathrm{c}} - l_{\mathrm{c}}^{m}$). It is evident that the leakage estimated by the data-driven approach is superior to the leakage from a model.

Publications

(http://www.gis.uni-stuttgart.de/research/publications/)

Refereed Journal Publications

Elmi, O., M. J. Tourian, and N. Sneeuw (2016b): Dynamic river masks from multi-temporal satellite imagery: an automatic algorithm using graph cuts optimization. In: *Remote Sensing*.

Ghobadi-Far, K., M. A. Sharifi, and N. Sneeuw (2016): 2D Fourier series representation of gravitational functionals in spherical coordinates. In: *Journal of Geodesy* 90 (9), pp. 871–881. DOI: 10.1007/s00190-016-0916-7.

Li, H., T. Reubelt, M. Antoni, and N. Sneeuw (2016): Gravity field error analysis for pendulum formations by a semi-analytical approach. In: *Journal of Geodesy*, pp. 1–19. DOI: 10.1007/s00190-016-0958-x.

Tourian, M. J., A. Tarpanelli, O. Elmi, T. Qin, L. Brocca, T. Moramarco, and N. Sneeuw (2016): Spatiotemporal densification of river water level time series by multimission satellite altimetry. In: *Water Resources Research* 52 (2), pp. 1140–1159. DOI: 10.1002/2015WR017654.

Vishwakarma, B. D., B. Devaraju, and N. Sneeuw (2016a): Minimizing the effects of filtering on catchment scale GRACE solutions. In: *Water Resources Research* (8), pp. 5868–5890. DOI: 10.1002/2016WR018960.

Ye, Z., R. Tenzer, N. Sneeuw, L. Liu, and F. Wild-Pfeiffer (2016): Generalized model for a Moho inversion from gravity and vertical gravity-gradient data. In: *Geophys. J. Int.* 207.1, pp. 111–128. DOI: 10.1093/gji/ggw251.

Poster Presentations

Domeneghetti, A., A. Tarpanelli, M. J. Tourian, L. Brocca, T. Moramarco, A. Castellarin, and N. Sneeuw (2016): *The Benefit of Multi-Mission Altimetry Series for the Calibration of Hydraulic Models*. EGU 2016, Vienna, Austria.

Elmi, O., M. J. Tourian, and N. Sneeuw (2016a): *An automatic water body area monitoring algorithm for satellite images based on Markov Random Fields*. EGU 2016, Vienna, Austria.

Javaid, M. A. and W. Keller (2016b): *Data mining for Monthly Spherical Harmonics (SH) Coefficients from GRACE satellite*. Second International Conference on Space, COMSTECH Secretariat, 33-Constitution Avenue, G-5/2, Islamabad, Pakistan.

Li, H., M. Antoni, T. Reubelt, N. Sneeuw, M. Zhong, and Z. Zhou (2016a): *Gravity Field Error Assessment for the Cartwheel Formation via the Semi-Analytical Approach*. 1st Joint Commission 2, IGFS Meeting, International Symposium on Gravity, Geoid, and Height Systems 2016, Thessaloniki, Greece.

Li, H., M. Antoni, T. Reubelt, N. Sneeuw, M. Zhong, and Z. Zhou (2016b): *A Semi-Analytical Approach to Gravity Field Analysis from Cartwheel Formation*. EGU2016, Vienna, Austria.

Li, H., M. Antoni, T. Reubelt, N. Sneeuw, M. Zhong, and Z. Zhou (2016c): *A Semi-Analytical Approach to Gravity Field Analysis from Cartwheel Formation*. GGHS 2016, Thessaloniki, Greece.

Liu, W., S. Iran Pour, M. J. Tourian, and N. Sneeuw (2016): *A data-driven method to calculate alias periods for de-aliasing ocean tide errors*. DAAD Thematic Network, Stuttgart, Germany.

Tourian, M. J., O. Elmi, Y. Shafaghi, and N. Sneeuw (2016): *HydroSat: a repository of global water cycle products from spaceborne geodetic sensors*. OSTS meeting 2016, La Rochelle, France.

Tourian, M. J. and N. Sneeuw (2016): *River discharge estimation from multi-mission altimetry with optimized spatial coverage and temporal resolution*. EGU 2016, Vienna, Austria.

Tourian, M. J., N. Sneeuw, M. Losch, and B. Rabe (2016): *Response of Arctic sea level and hydrography to hydrological regime change over boreal catchments*. EGU 2016, Vienna, Austria.

Vishwakarma, B. D., B. Devaraju, and N. Sneeuw (2016c): *Repairing filtering-induced damage to GRACE signal at catchment scale*. ESA Living Planet Symposium 2016, Prague, Czech Republic.

Vishwakarma, B. D. and N. Sneeuw (2016): *Reducing the filtering-induced error in Greenland ice mass loss seen by GRACE*. ESA Living Planet Symposium 2016, Prague, Czech Republic.

Vishwakarma, B. D., N. Sneeuw, and B. Devaraju (2016): *Repairing filtering induced damage to the GRACE time-series at catchment scale*. EGU 2016, Vienna, Austria.

Zhang, J. and N. Sneeuw (2016): *Common patterns of continental water storage and sea surface temperature*. DAAD Thematic Network Workshop 2016, Stuttgart, Germany.

Conference Presentations

Ghobadi-Far, K., M. Sharifi, and N. Sneeuw (2016): *2D Fourier series representation of gravity quantities on the sphere*. 1st Joint Commission 2, IGFS Meeting, International Symposium on Gravity, Geoid, and Height Systems (GGHS 2016), Thessaloniki, Greece,

Grafarend, E. W. (2016a): *The Geodetic Anholonomity Problem*. 609. WE-Heraeus-Seminar: Relativistic Geodesy: Foundations and Applications, Physikzentrum Bad Honnef.

Grafarend, E. W. (2016b): *Wissenschaftlicher Diskurs zu Friedrich Robert Helmert*. Wissenschaftliches Kolloquium Helmert-Turm, GFZ, Potsdam, Germany.

Javaid, M. A. and W. Keller (2016a): *Comparison of two gravity recovery algorithms based on the variational equation approach*. Second International Conference on Space, COMSTECH Secretariat, 33-Constitution Avenue, G-5/2, Islamabad, Pakistan.

Kunstmann, H., C. Lorenz, M. J. Tourian, B. Devaraju, and N. Sneeuw (2016): *Basin-scale runoff prediction: An Ensemble Kalman Filter framework based on global hydrometeorological data sets*. EGU 2016, Vienna, Austria.

Li, J., N. Sneeuw, W. Jiang, J. Cai, Y. Chu, and T. Jin (2016): *The lake level monitoring in China from satellite altimetric missions*. Dragon 3 Final Results Symposium, Wuhan.

Liu, W., N. Sneeuw, S. Iran Pour, W. Jiang, M. J. Tourian, and T. Reubelt (2016): *Ocean tide aliasing in spaceborne gravimetry: a data-driven determination of the tidal alias spectrum*. International Symposium on Gravity, Geoid and Height Systems 2016, Thessaloniki, Greece.

Sneeuw, N. (2016a): *Future satellite gravimetry missions: recent developments in Europe as well as algorithmic aspects*. Chinese Academy of Surveying and Mapping (CASM), Beijing, PR China).

Sneeuw, N. (2016b): *Future satellite gravimetry missions: recent developments in Europe as well as algorithmic aspects*. Huazhong University of Science and Technology, Center of Gravitational Experiments (CGE), Wuhan, PR China).

Sneeuw, N. (2016c): *Future satellite gravimetry missions: recent developments in Europe as well as algorithmic aspects*. Wuhan University, School of Geodesy & Geomatics, Wuhan, PR China.

Sneeuw, N., S. Iran Pour, T. Reubelt, I. Daras, M. Murböck, R. Pail, T. Gruber, P. Visser, J. Encarnação, J. van den IJssel, T. Van Dam, M. Weigelt, S. Cesare, S. Tonetti, S. Cornara, R. Haagmans, C. Siemes, and L. Massotti (2016): *ESA SC4MGV Study: Assessment of Satellite Constellations for Monitoring the Variations in Earth Gravity Field*. ESA Living Planet Symposium 2016, Prague, Czech Republic.

Sneeuw, N. and J. Li (2016): *Monitoring lake level variations over the Qinghai-Tibet Plateau by consistent multi-satellite altimetry (QTibMSA)*. Dragon 4 Kick-Off Symposium, Wuhan, China.

Sneeuw, N., J. Li, J. Cai, W. Jiang, M. Tourian, O. Elmi, Y. Chu, and T. Jin (2016): *Current and future geodetic satellite missions for global change monitoring*. Dragon 3 Final Results Symposium, Wuhan, China.

Tourian, M. J., O. Elmi, and N. Sneeuw (2016): *Combining the strength of satellite altimetry and imagery to estimate river discharge*. OSTS meeting 2016, La Rochelle, France.

Tourian, M. J., J. Riegger, and N. Sneeuw (2016): *GRACE, 14 years monitoring of the water storage anomaly: how about quantification of total drainable water storage?* Geodetic Week 2016, Hamburg, Germany.

Vishwakarma, B. D., L. Balangé, N. Sneeuw, and B. Devaraju (2016a): *Hydro-meteorological validation of GRACE de-leakage approach*. Geodetic Week 2016, Hamburg, Germany.

Vishwakarma, B. D., L. Balangé, N. Sneeuw, and B. Devaraju (2016b): *Minimizing filtering induced change to GRACE signal at catchment scale*. International Symposium on Gravity, Geoid and Height Systems 2016, Thessaloniki, Greece.

Books & Miscellaneous

Sneeuw, N., P. Novák, M. Crespi, and F. Sansò, eds. (2016). Vol. 142. IAG Symposia. Springer Verlag, Berlin Heidelberg, Germany. DOI: 10.1007/978-3-319-30530-1.

Tourian, M., R. Thor, and N. Sneeuw (2016): "Least-Squares Prediction of Runoff Over Ungauged Basins". In: *IAG 150 Years – Proceedings of the IAG Scientific Assembly in Postdam, Germany, 2013*. Ed. by C. Rizos and P. Willis. Vol. 143. IAG Symposia. Springer, pp. 257–261. DOI: 10.1007/1345_2015_170.

Master Theses

(http://www.gis.uni-stuttgart.de/edu/theses/finished_theses/)

Wen Huang: Analysis of GNSS Inter-satellite Networks

Wei Liu: Ocean tide de-aliasing for future gravity missions

Bachelor Theses

(http://www.gis.uni-stuttgart.de/edu/theses/finished_theses/)

Laura Balangé: Validation of GRACE products by closing the water budget

Tatjana Immel: Ausflussbestimmung aus Satellitenaltimetrie und Fernerkundung - eine Fehleruntersuchung

Philipp Luz: Digitalisierung von Liegenschaftskatasterakten

Guest Lectures and Lectures on special occasions

I. N. Tziavos (Aristotle University of Thessaloniki): Gravity field research at the Aristotle University of Thessaloniki, The GeoGrav scientific group (25.4)

L. Sjöberg (Royal Institute of Technology (KTH), Stockholm, Schweden): Least Square Modification of Stokes? Formula vs. Remove-Compute-Restore Technique (24.11.)

Lectures at other universities

Sneeuw N: Höhere Erdmessung: Historisch-mathematische Entwicklungen von Bruns bis Kaula und weiter, Braunschweigische Wissenschaftliche Gesellschaft, Braunschweig (29.4.)

Sneeuw N: Future satellite gravimetry missions: recent developments in Europe as well as algorithmic aspects, Huazhong University of Science and Technology, Center of Gravitational Experiments (CGE), Wuhan, PR China (2.11.)

Research Stays

Grafarend E.:
Finnish Geodetic Research Institute, Masala/Helsinki, Finland (10.8.-6.9.)

Activities in National and International Organizations

Grafarend E.
Professor h.c., University of Navarra, Pamplona, Spain
Professor h.c., University of Tehran, Iran Professor h.c., Wuhan University, China Elected Member of the Finnish Academy of Sciences and Letters, Finland
Elected Member of the Hungarian Academy of Sciences, Hungary
Member Royal Astronomical Society, Great Britain
Corresponding Member Österreichische Geodätische Kommission (ÖGK)
Member Flat Earth Society
Fellow International Association of Geodesy (IAG)
Emeritus Member German Geodetic Commission (DGK)
Gauss Society, Göttingen
Member of the ”Leibniz Gesellschaft der Wissenschaften”, Berlin

Sneeuw N.
Full Member Deutsche Geodätische Kommission (DGK)
Adjunct Professor of the College of Engineering, University of Tehran, 03.2015–02.2017
Member Editorial Board of Studia Geophysica et Geodaetica
Member Editorial Board of Surveys in Geophysics
Fellow International Association of Geodesy (IAG)

Courses – Lecture/Lab/Seminar

Advanced Mathematics (Keller, Antoni)	3/2/0/0
Aktuelle Geodätische Satellitenmissionen (Sneeuw)	2/2/0/0
Amtliches Vermessungswesen und Liegenschaftskataster (Steudle)	2/0/0/0
Amtliche Geoinformation (Heß)	2/0/0/0

Ausgewählte Kapitel der Parameterschätzung (Krumm, Roth)	2/2/0/0
Ausgleichungsrechnung I, II (Krumm, Roth)	3/1/0/0
Dynamische Erdmodelle (Tourian)	0/2/0/0
Dynamische Satellitengeodäsie (Sneeuw, Tourian)	1/1/0/0
Einführung Geodäsie und Geoinformatik (Sneeuw)	2/2/0/0
Foundations of Satellite Geodesy (Keller)	2/1/0/0
Integriertes Praktikum/Integrated Field Work (Keller, Sneeuw)	10 days
Koordinaten- und Zeitsysteme in der Geodäsie (Sneeuw)	2/2/0/0
Landesvermessung (Krumm, Roth)	2/2/0/0
Map Projections and Geodetic Coordinate Systems (Krumm, Roth)	2/1/0/0
Physikalische Geodäsie (Engels, Tourian)	2/2/0/0
Referenzsysteme (Krumm, Roth)	2/2/0/0
Satellitengeodäsie (Sneeuw, Tourian)	2/1/0/0
Satellitengeodäsie (Keller, Tourian)	1/1/0/0
Satellite Geodesy Observation Techniques (Keller, Tourian)	2/1/0/0
Statistical Inference (Krumm, Roth)	2/1/0/0
Wertermittlung I, II (Bolenz)	4/0/0/0

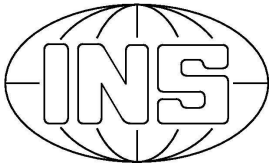

Institute of Navigation

Breitscheidstrasse 2, D-70174 Stuttgart,
Tel.: +49 711 685 83400, Fax: +49 711 685 82755
e-mail: ins@nav.uni-stuttgart.de
homepage: http://www.nav.uni-stuttgart.de

Head of Institute

Prof. Dr.-Ing. Alfred Kleusberg

Deputy: Dr.-Ing. Aloysius Wehr
Secretary: Helga Mehrbrodt

Staff

Dipl.-Ing. Doris Becker	Navigation Systems
Dipl.-Ing. Michael Gäb	Navigation Systems
Dipl.-Geogr. Thomas Gauger	GIS Modelling and Mapping
Dipl.-Ing. René Pasternak	Remote Sensing
Dipl.-Ing. Bernhardt Schäfer	Navigation Systems
Dipl.-Ing. (FH) Martin Thomas	Laser Systems
Dr.-Ing. Aloysius Wehr	Laser Systems
Dr. Ing. Franziska Wild-Pfeiffer	Navigation Systems

EDP and Networking

Regine Schlothan

Laboratory and Technical Shop (ZLW)

Dr.-Ing. Aloysius Wehr (Head of ZLW)
Technician Peter Selig-Eder
Electrician Sebastian Schneider
Mechanician Master Michael Pfeiffer

External teaching staff

Hon. Prof. Dr.-rer.nat. Volker Liebig - Directorate ESA
Hon. Prof. Dr.-Ing. Hans Martin Braun - RST Raumfahrt Systemtechnik AG, St.Gallen
Dr. Werner Enderle - Europäisches Satelliten Kontrollzentrum (ESOC), Darmstadt

Research Projects

Redesign and Extension of the Experimental 3D-Printer for Housing Fabrication and Printing 3D-Laser Scanner Data

The Experimental 3D-Printer (E3DP) presented in the annual report 2015 already demonstrated that this technology can well be used for printing figures and models derived from 3D-laser scanner data. However, the carried out experiments made clear that the achieved printing accuracy did not fit the requirements specified by the design drawings of e.g. the small housings of wearable electronics and housings for special electronics. Furthermore, the printer worked not reliable and needed intensive supervision, which made printing e.g. overnight impossible. An unsupervised printing is desired, because the printing of larger objects can last hours. First the mechanical setup was redesigned under the objectives mechanical stability and stiffness of the construction. Accompanying strength calculations clearly showed, which parts of the printer had to be redesigned. To minimize vibrations caused by the stepping motors and other mechanical moving parts and to relax the alignment requirements of the drive trains, belt drives were selected for each printing axis. Further tests made clear that the extruder heater needed an optimization and a special cooling system at its output nozzle. Meanwhile the design has matured so that the cooling system could be printed by E3DP itself. Also, the stepping motor flanges were realized in poly-lactic acid (PLA) material by using E3DP. This reduced drastically the acoustic drive noise. Although, this material has not got the stiffness of aluminum, accuracy degradation was not observed, due to the design regarding stiffness.

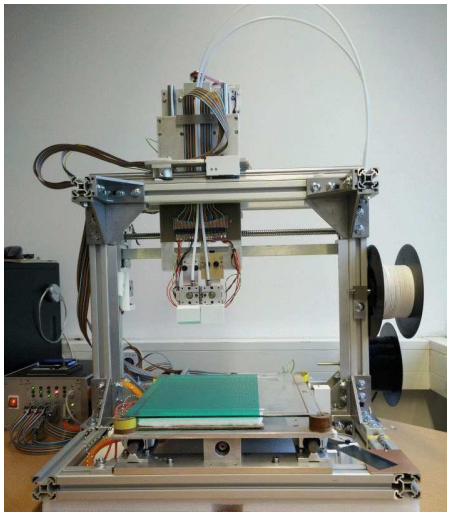

Figure 1: Redesigned E3DP with two extruders.

The redesigned E3DP achieved the desired accuracy. However, an unsupervised print was not possible, because very often some areas of the first printed layer detached from the heated glass plate, although, several layers had been already printed above the ground layer. This caused a collision of the nozzle with the object and the print process had to be canceled.

Studies concerning this fact depicts that objects covering a larger ground area tended to detach more easily especially at the corners. As the detaching was dependent on the object size the vertical deformation of the glass plate was measured. The measurement showed that the glass plate behaved like a membrane which elevated and settled in dependence on the temperature. The elevation swing was about one tenth of a millimeter with a time interval of five seconds, although a closed loop temperature control was used. The elevation difference of 0.1mm was proportional to the temperature difference of 0.1K measured in the control loop. This temperature difference is the error of the temperature control loop. As the glass plate was heated by a heating foil underneath the glass plate, which did not offer an equal heat distribution, and glass had got a very low thermal conductivity, thermal strains arose inside the glass plate which caused the observed deformation. Now, an aluminum heating plate is used. Aluminum has a 260 times higher thermal conductivity than glass. There is still a deformation of about 0.06mm at 60^{o} C, which is the working temperature. However, this value remains constant, if the heating control loop works within the specified limits of 0.1 K.

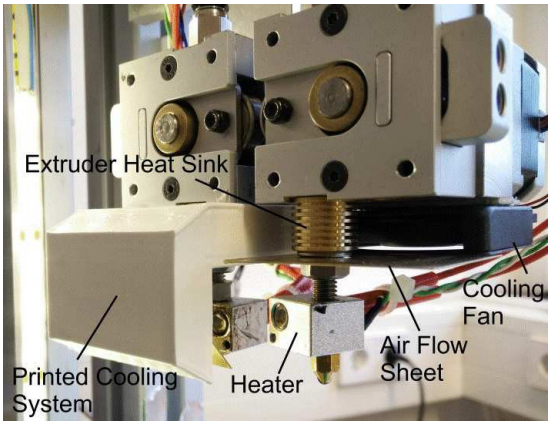

Figure 2: Extruder heating and cooling system.

The optimized and operational E3DP is shown in Figure1. It is equipped with two extruders. This makes possible to print either two PLA filaments with different colors or PLA filament and an additional special filament as supporting material for realizing bigger cavities inside the body. Figure 2 shows the extruder cooling system printed by E3DP and the optimized extruder heating part. Figure 3 depicts the stepping motor flange printed by E3DP.

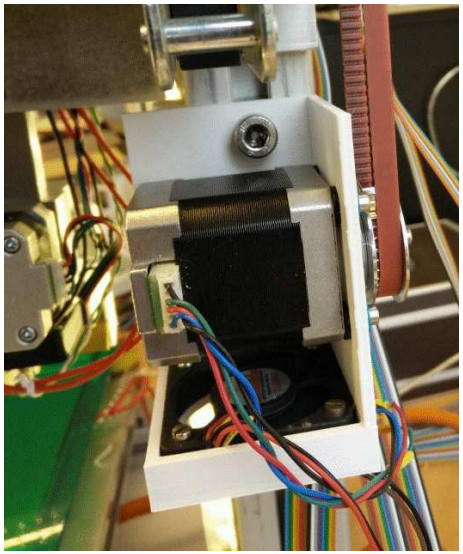

Figure 3: Printed stepping motor flange (white) and belt drive.

The printer exhibits the following technical data:

- ▷ print volume: 290 mm x 290 mm x 185 mm
- ▷ accuracy: 0.1 mm
- ▷ print material: PLA (diameter 1.75 mm)
- ▷ extruder nozzle diameter: 0.4 mm
- ▷ print file format:STL (STereoLithography, Standard Tessellation Language)

Analysis and Correction of Data Sets of Nitrogen Deposition in Baden-Württemberg Contributing to a Country Specific Nitrogen Balance

The project „Application of modelled nitrogen deposition 2007/2009 for ecosystems in Baden-Württemberg“ funded by Baden-Württemberg was finalised. Within the project maps of the national BMU/UBA „PINETI 2“ exercise (Pollutant Input and EcosysTem Impact; BMU/UBA FE-No 3712 63 240-1) were compiled, analysed and corrected. Since „PINETI 2“ modelling results of anthropogenic nitrogen dry deposition, modelled using the chemical transport model LOTOS-EUROS, are severely underestimating measurements of total nitrogen input into sensitive forest ecosystems in Baden-Württemberg, it was decided to develop and apply a methodology to correct „PINETI2“ deposition data fields in order to be in line with empirical „ground truth“ data based on measurements available at about 20 forest plots in Baden-Württemberg.

The correction procedure is carried out using geo-statistical GIS application in order to derive high resolution maps (1 ha grid) of ecosystem specific nitrogen deposition. In south-west Germany the complex orographic situation to some extent is determining the magnitude of nitrogen total deposition flux on a small scale. The co-kriging technique applied enables accounting for these local phenomena by making use of high resolution digital elevation model data together with dry deposition estimates derived using canopy budget calculations based on high quality data measured at 20 forest plots in Baden-Württemberg for modelling nitrogen deposition maps. The calculation for non-forest ecosystems relies on LOTOS-EUROS model calculations. Thus the spatial distribution of ecosystem specific deposition fluxes is preserved, while the deposition levels are adjusted to the routinely measured deposition data (Figure 4).

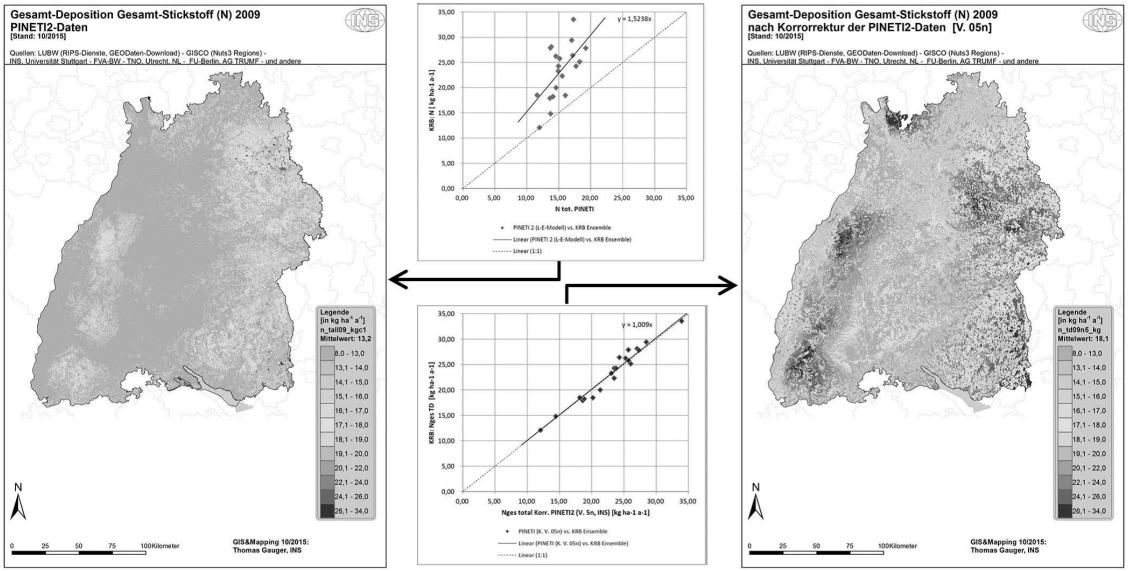

Figure 4: Total deposition of reactive nitrogen in Baden-Württemberg 2009: BMU/UBA „PINETI 2“ model output (left); map corrected using forest measurement data (right); the scatter plots (middle) are comparing the respective maps (x-axis) with respect to empirical N deposition estimates at coniferous forest plots (y-axis) to which the „PINETI 2“ model output (left map) was adjusted (right map). [Data Sources: BMU/UBA 37126340-1, FVA-BW LUBW and others]

The project results are of interest for Baden-Württemberg, because these data are supporting EU and national regulations on air pollution control and emission abatement (EU NEC directive, BImSchG, TA-Luft), which have to be implemented on the sub-national level of the federate states of Germany. Moreover, scientific interest is supported by these data, e.g. when setting up flux assessment studies within certain ecosystems, ecological impact assessment, biodiversity, and

nature protection. Administrative applications aiming at emission control and emission reduction of air pollutants are using the mapped nitrogen deposition data with reference to permission of projected animal husbandry, road construction, industrial settlements, and power plants, respectively. Hence the project results of nitrogen deposition are designated for public use and are accessible via the internet at LUBW (www.fachdokumente.lubw.baden-wuerttemberg.de/ > Umweltbeobachtung > ID U46-S7-J16).

A follow-up research project funded by Landesanstalt für Umwelt, Messungen und Naturschutz Baden-Württemberg (LUBW) is launched at the end of 2016, combining different modelling approaches in order to derive actual high resolution maps of air concentration and deposition of reactive nitrogen species for Baden-Württemberg. Where ever possible the use of measurement data is integrated into the modelling approach. A consortium was set up for carrying out the joint research consisting of Meteotest, Bern (CH), EURAD group of Rhenish Institute for Environmental Research at the University of Cologne (RIU), Interra, Büro für Umweltmonitoring, Kenzingen, and INS as project leader, beyond that close co-operation is arranged with LUBW, FVA-BW, Ingenieurbüro Lohmeyer, Radebeul, and TNO, Utrecht (NL).

Publications and Presentations

Ye, Z.; Tenzer, R.; Sneeuw, N.; Liu, L and Wild-Pfeiffer, F.: Generalized model for a Moho inversion from gravity and vertical gravity-gradient data, Geophysical Journal International, 2016, vol. 207, no. 1, 111-128, doi: 10.1093/gji/ggw251.

Bachelor Thesis

Evaluierung des Integrierten Navigationssystems POS LV (Becker).

Master Thesis

Evaluation of the „low-cost“ GNSS-Receiver ublox NEO-7P (Becker).

Classification of Multi-Temporal TerraSAR-X Data with the Help of an Object-Based Approach (Pasternak).

Pixel-based Classification of Multi-Temporal TerraSAR-X Data in Eastern Part of Kraichgau Region (Pasternak)

Activities in National and International Organizations

Alfred Kleusberg Fellow of the International Association of the Geodesy
Member of the Institute of Navigation (U.S.)
Member of the Royal Institute of Navigation
Member of the German Institute of Navigation

Education (Lecture / Practice / Training / Seminar)

Introduction of Geodesy and Geoinformatic (BSc) (Kleusberg, Schäfer)	2/2/0/0
Electronics and Electrical Engineering (Wehr)	2/1/0/0
Satellite Measurement Engineering (Wehr)	2/1/0/0
Parameter Estimation in Dynamic Systems (Kleusberg)	2/1/0/0
Navigation I (Kleusberg, Gäb)	2/2/0/0
Inertial Navigation (Kleusberg, Schäfer)	2/2/0/0
Remote Sensing I (Wild-Pfeiffer, Pasternak)	2/2/0/0
Remote Sensing I (BSc) (Wild-Pfeiffer, Pasternak)	2/1/0/0
Remote Sensing II (Wild-Pfeiffer, Pasternak)	1/1/0/0
Satellite Programs in Remote Sensing, Communication and Navigation I (Liebig)	2/0/0/0
Satellite Programs in Remote Sensing, Communication and Navigation II (Liebig)	2/0/0/0
Radar Measurement Methods I (Braun)	2/0/0/0
Radar Measurement Methods II (Braun)	2/1/0/0
Dynamic System Estimation (Kleusberg)	2/1/0/0
Integrated Positioning and Navigation (Kleusberg, Schäfer)	2/1/0/0
Satellite Navigation (Kleusberg)	2/1/0/0
Interplanetary Trajectories (Becker)	1/1/0/0
Geodetic Seminar I, II (Fritsch, Sneeuw, Keller, Kleusberg, Möhlenbrink)	0/0/0/4
Integrated Fieldwork (Pasternak,Schäfer)	(SS 2016)

Institute for Photogrammetry

Geschwister-Scholl-Str. 24D, D-70174 Stuttgart
Tel.: +49 711 685 83386, Fax: +49 711 685 83297
e-mail: firstname.secondname@ifp.uni-stuttgart.de
url: http://www.ifp.uni-stuttgart.de

Head of Institute

Prof. Dr.-Ing. Uwe Sörgel

Deputy:	apl. Prof. Dr.-Ing. Norbert Haala
Personal Assistant:	Martina Kroma
Emeritus Professors:	Prof. Dr.-Ing. Dr. hc. mult. Fritz Ackermann
	Prof. Dr.-Ing. Dieter Fritsch

Research Groups at the ifp

Geoinformatics

Chair: Dr.-Ing. Volker Walter	
Deputy: Dr.-Ing. Susanne Becker	Point Cloud Interpretation and Hybrid GIS
MSc. Lavinia Runcenau	Modelling of Building Interiors
Dipl.-Ing. Patrick Tutzauer	Façade Reconstruction, Interpretation and Modelling

Photogrammetric Computer Vision

Chair: apl. Prof. Dr.-Ing. Norbert Haala	
Dr.-Ing. José Balsa-Barreiro	Cultural Heritage
Dipl.-Ing. Alessandro Cefalu	Photogrammetric Calibration and Object Recognition
M.A. Chance Michael Coughenour	Remote Sensing Applications to Archaeology

Photogrammetric Systems

Chair: Dr.-Ing. Michael Cramer	
Dipl.-Ing.(FH) Markus Englich	Sensor Laboratory, Computing Facilities

Remote Sensing

Chair: apl. Prof. Dr.-Ing. Uwe Sörgel	
MSc. Chia-Hsiang Yang	Persistant Scatterer Interferometry

Stipendiaries and external PhD Students

MSc. Stefan Cavegn	Image-based Mobile Mapping
MSc. Ke Gong	3D Reconstruction
Dipl.-Ing. Wolfgang Groß	Transformation of Hyperspectral Data
Dipl.-Phys. Hendrik Schilling	Classification of Hyperspectral Data
MSc. Mehrdad Nekouei Sharaki	Photogrammetric Image Processing

Guests

Dr. Haiyan Gu	Image Analysis
MSc. Jyun-Ping Jhan	Photogrammteric Image Processing

External Teaching Staff

Dipl.-Ing. Stefan Dvorak, Amt für Stadtentwicklung und Vermessung, Reutlingen

Research Projects

Geoinformatics

Building Category Classification from Crawled Urban Data

Recent years have shown a shift from pure geometric 3D city models to data with semantics. This is, among others, induced by applications and requirements like Building Information Modelling (BIM) and Smart Cities. We investigate in bridging this gap by proposing a pipeline to use crawled urban imagery and link it with ground truth cadastral data as an input for automatic building use classification. Semantic information as required for a multitude of applications like urban planning and infrastructure management includes building use, number of dwelling units and so on. A key information, from which several other metrics can be derived or at least be approximated, is the aforementioned building use. We aim to extract this information automatically from Street View (SV) imagery. Convolutional Neural Networks (CNNs) proved to be extremely successful for image interpretation, however, require a huge amount of training data. Therefore, we try to automatically generate such training datasets by linking semantic information as already available from databases provided from national mapping agencies or city administrations to the corresponding façade images extracted from SV.

To extract only building-relevant parts from the Street View data, the images are pre-processed. Therefore, we utilize metadata provided by the Street View API and take advantage of a Deep Learning framework for semantic image segmentation to analyse our data for relevant content.

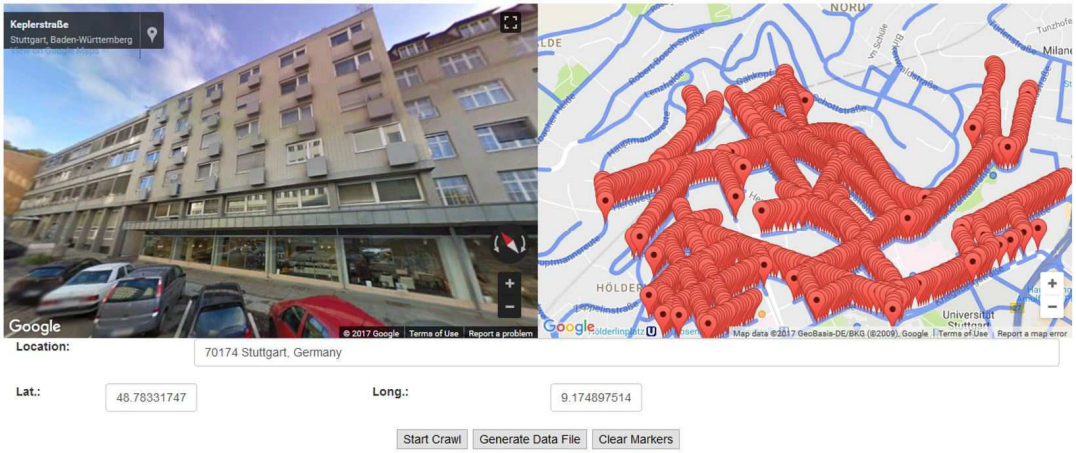

Figure 1: Street View Crawling interface. Left: Initial Crawling position. Right: Each crawled position depicted by a marker.

Based on the information obtained in the crawling process we try to link image content with building polygons in the ground truth. The outcome is a tuple of building images and its corresponding building category. This data is then used to train a classifier. With the trained classifier, it is possible to predict building categories for new input images.

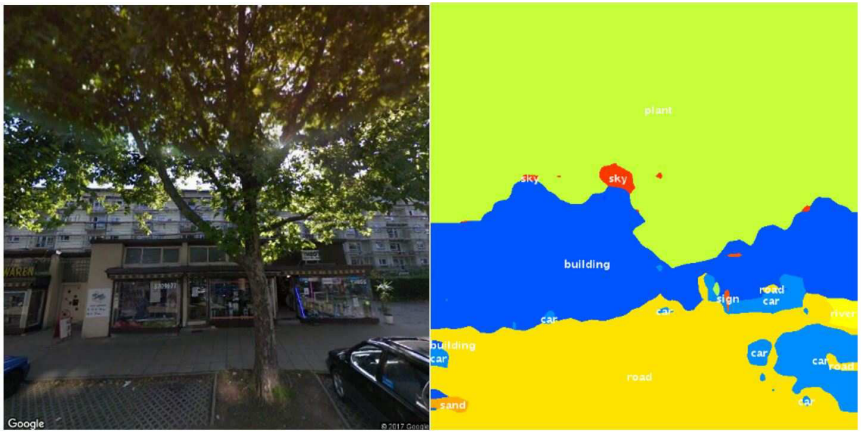

Figure 2: Semantic segmentation of SV images to discard unsuitable candidates. This example would be discarded due to large occlusions by vegetation.

Building category information is also beneficial for a better visual understanding of virtual city models. If the usage type is known for every building, perceptual constraints can be used to manipulate the geometry of the model in a way that its building category is recognizable more easily. Therefore, we performed a follow-up user study to our first one from last year to better understand human perception of different building categories. Here, users were confronted with buildings of different representation types (Textured Mesh, Untextured LOD3 Model) in a 3D environment where they could freely zoom, rotate and pan the models and subsequently should classify them into the assumed building category.

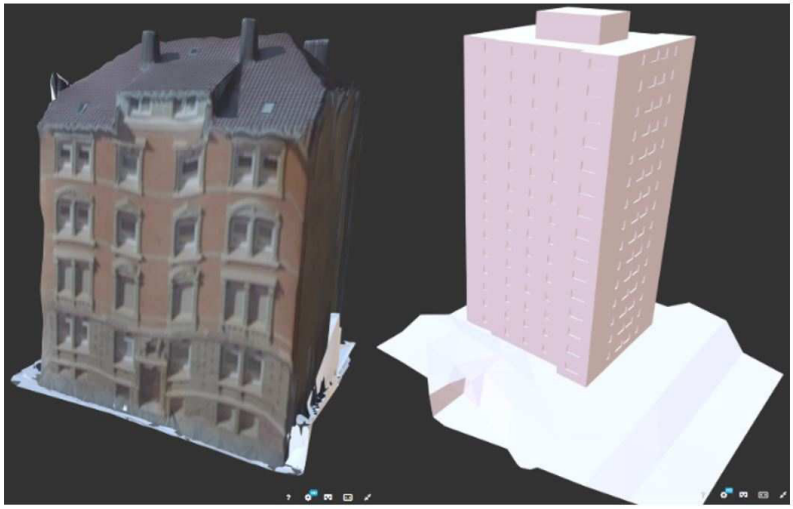

Figure 3: Different building types presented to the user in a 3D environment web interface.

Use Cases for grammar-supported crowd-sourced 3D indoor modeling

In our previous work, we developed a formal grammar to support crowd-sourced 3D indoor modeling. Reflecting the fact that a building can be analyzed from coarse to fine (e.g., separation of a building into floors, separation of a floor into hallway and non-hallway, separation of non-hallway into rooms, identify different objects within a room), the grammar covers several hierarchical levels: floor - floor (Split Grammar), hallway - non-hallway (L-System), room - room (Split Grammar), room - interior (Extended Grammar). Using this grammar concept, a system architecture has been worked out (see Figure 4) based on which several uses cases can be defined.

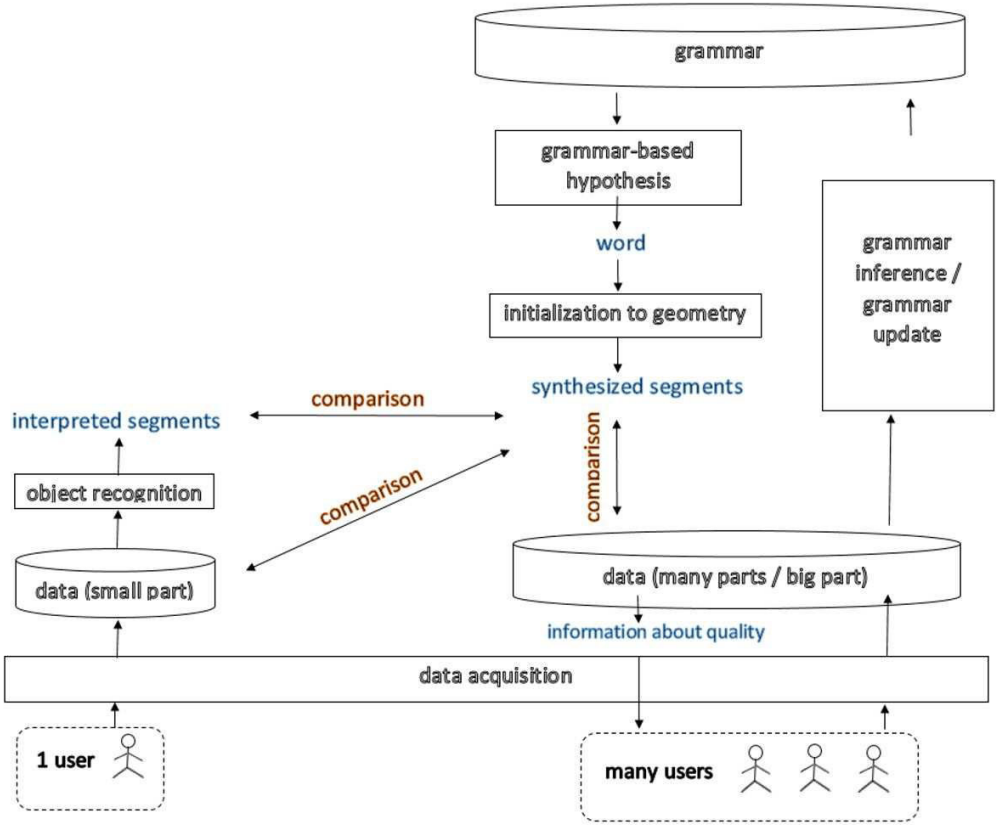

Figure 4: System architecture for grammar-supported crowd-sourced 3D indoor modeling.

Use case: „grammar inference“

In this scenario, the grammar development is realized, based on a sufficient big data set acquired by many users. It is expected that the individual parts of the data have a considerable overlap with the others. The grammar inference is realized by hierarchically interpreting the data and deriving the needed input and rules for each grammar level. For the hierarchical detection of primitives, object detection algorithms are used. The grammar is built in a way that ensures inter-connectivity between the geometry and the semantics. Furthermore, connections should exist between the different grammar levels. The grammar is able to generate hypotheses for the different hierarchical levels. The hypotheses are influenced by the probabilities of the rules. These probabilities are computed considering how often a rule was used.

Use case: „grammar update“

In this scenario, the initially learned grammar is updated. The available model is compared with the new acquired data, and most probably conflicts will result. The conflicts mean inconsistencies between predicted (hypotheses coming from grammar) and newly detected geometry or semantics. In order to solve these conflicts, the probabilistic confidence of rules might describe their quality. Fuzzy logic could also be a solution for expressing the quality of the grammar rules. If the resolution of the conflict results in a higher confidence of the new data, the grammar update is realized. From interpreting the new data, new rules are built. Therefore, the existing rules are updated with the new ones.

Use case: „smart hierarchical object interpretation“

In this scenario, the grammar is already known, and one user acquires a small data set. In the new data set, object recognition algorithms, with grammar support, are used for detecting the grammar primitives. At the beginning, the grammar support means very rough information about the primitives that one should search for. As an example, initially, one can search for planes in the data set. The primitives found in the data, the interpreted data segments, are compared with the synthesized segments delivered by the grammar hypotheses. Through this comparison, one could find the most likely segments by selecting from the synthesized segments the ones which correspond to the segments identified from the data set. In the same time, one can identify the grammar level needed in order to detect the specific rules to be further applied.

Use case: „optimized sensing“

In this scenario, the grammar is available. By comparing the model proposed by the grammar with the building shell, a quality analysis is performed delivering some completeness indicators. This information is send to the users as a request for acquiring more data and also the location where they should measure.

Indoor point cloud segmentation for automatic object interpretation

A large variety of systems and applications are offering mapping, localization and navigation services for outdoor environment. However, people spend most of their time indoor, where there is a lack in digital maps and where conventional GPS services do not work. Despite this need in indoor navigation applications, the developments in the field of augmented and virtual reality, including also game industry, and Building Information Modelling (BIM), are also requiring intelligent indoor models.

In order to obtain the needed models, innovative equipment is required to replace the traditional systems, which are mostly expensive and sometimes inconvenient to use. Recently, a variety of systems, designed for this purpose, were made available on the market. In order to increase the mapping efficiency and in the same time to reduce the mapping costs, these systems integrate

laser scanners, cameras and sometimes inertial measurement units. Also, they adapt their design to the indoor space, being built as a trolley or as a backpack (e.g. NavVis M3 Trolley, Leica Pegasus). Another step further is made by the availability, at a consumer-level, of devices integrating depth cameras. These platforms are using low cost sensors which made them affordable to the general public (e.g. Phab 2 Pro Phone, Google Tango Tablet, Microsoft Kinect).

All this progress enables unexperienced users to contribute to the indoor mapping request, but in the same time this rises new challenges which need to be overcome. The acquired 3D data needs to be automatically interpreted in order to obtain the models for the aforementioned applications. For the automatic 3D data interpretation, segmentation is needed. Point cloud segmentation is a subject of research for many years, however point clouds coming from low cost sensors, rise new challenges for the segmentation and interpretation process, which were addressed by us.

For automatically interpreting 3D indoor data, it was considered an indoor dataset acquired with Google Tango Tablet and it was analysed and interpreted in parallel with data, of the same indoor space, coming from NavVis M3 Trolley (Figure 5). A terrestrial laser scanner (TLS) point cloud was considered to be the reference.

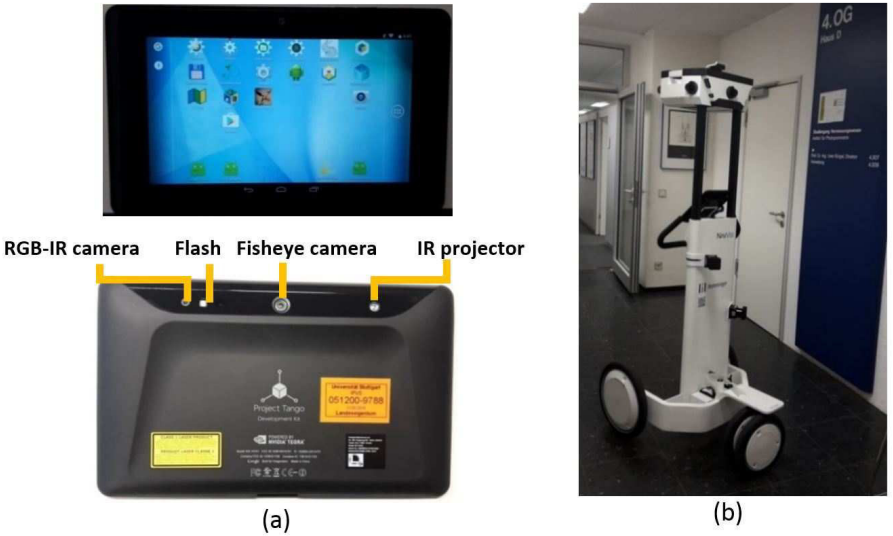

Figure 5: (a) Google Tango tablet; (b) NavVis M3 trolley.

In the first part of the proposed algorithm, a pre-processing step was needed for preparing the data acquired with Google Tango Tablet for the segmentation. Considering that the errors coming with the data, acquired with low cost sensors, are strongly influencing the later processing, a

sparse outlier removal algorithm was applied. For making the further process more efficient, a downsampling method based on voxel grid filtering, was used. Some data irregularities were eliminated with the help of a resampling algorithm.

In a second step, it was aimed to distinguish between the large variety of indoor objects, such as walls, chairs, tables, cupboards, etc., and for this reason different algorithms should be used, adapted to the object to be detected. Region based methods are suitable to differentiate between different objects, but it cannot detect if the resulted regions are containing the same object type. As a first step in modelling the 3D interior, walls were aimed to be detected. Therefore, the 3D points were filtered under a specific height, in order to remove the furniture. The remaining points after filtering were clustered in different wall segments by applying a model-based segmentation algorithm. We proposed an iterative RANSAC method. The detected wall segments were passed through a filtering process, eliminating the ones which do not fulfil the architectural conditions (e.g. are forming very small angles with other detected walls, or are located too close to another wall).

The proposed algorithm is very flexible, not being restricted to the Manhattan World constrains, and accurate enough to detect the main wall structures. However, problems could appear due to the noisy and incomplete character of the data.

These problems were revealed by applying the proposed wall segmentation algorithm again on a more accurate dataset acquired with the NavVis M3 Trolley. By referring these datasets to a reference TLS dataset made also possible an accuracy analysis of the previous detected wall segments. Some of the detected wall positions proved to be displaced, this being not influenced by the algorithm used, but of the noisy character of the data and possible remaining registration errors (Figure 6).

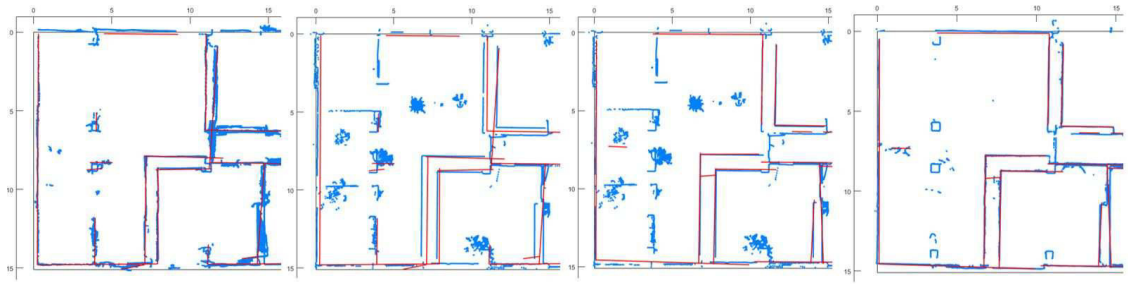

Figure 6: Detail of detected wall segments from: (a)Tango tablet and Tango tablet point cloud; (b) Tango tablet and TLS point cloud; (c)M3 trolley and TLS point cloud; (b) M3 trolley point cloud and M3 trolley point cloud.

On the one side, for some of the indoor navigation applications the existing wall displacement will be tolerated. On the other side, a way to overcome these problems is to use a formal grammar for modelling the indoor environment. The results of the interpretation step will be used as a knowledge base for automatically inferring the grammar rules. Assuming that the 3D point cloud is already registered within the building shell, the relative position of the wall segments will be used also for obtaining the grammar parameters and constrains.

Photogrammetric Computer Vision

Hierarchical Structure from Motion combining global Image Orientation and structureless Bundle Adjustment

Global image orientation techniques aim at estimating camera rotations and poses for a whole set of images simultaneously. One of the main arguments for these procedures is an improved robustness against drifting of camera stations in comparison to more classical sequential approaches. Usually, the process consists of computation of global rotations and, in a second step, global positions for the cameras. Depending on the approach, either the first or both steps rely on the network of transformations arising from relative orientations between cameras. Therefore, the quality of the obtained global results is influenced by tensions in the network. These may e.g. be induced by insufficient knowledge of the intrinsic camera parameters. Another reason can be found in local weaknesses in the connectivity. We suggest hierarchical subdivision with intermediate bundle adjustment to reduce these effects. We adopt an efficient global technique which registers triplets based on fixed global camera rotations and scaled relative camera translations but does not involve scene structure elements in the fusion step. In contrast, our variant works with arbitrarily sized and oriented subsets of the full dataset, by computing relative rotations between - and subsequently global rotations for - submodels and is applied hierarchically. Furthermore we substitute classical bundle adjustment by a structureless approach basing on epipolar geometry and augmented by a scale consistency constraint which we derive from law of sines.

Given a connectivity graph and relative orientations between image pairs, our approach proceeds over global rotations to a RANSAC based estimation of camera positions for selected triplets of images. Keeping the rotations fixed, we estimated the positions forcing points to be triangulated in front of the image plane. The triplets form the lowest level of submodel hierarchy. Iteratively, we grow every submodel of the current hierarchy level by connecting neighbouring submodels (two or more shared cameras) to define the models of the next level. Only unique submodels are kept. A further selection scheme, which builds upon a connectivity measure between submodels is applied to reduce the number of created models. For submodels selected to be fused to next level models, we compute relative rotations using the global (w.r.t. the corresponding submodel) rotations of shared cameras and use these to compute global rotations for the submodels. Fixing these rotations, global poses for the cameras are estimated based on the relative translations of shared cameras and a single scale parameter for every submodel as indicated in Figure 7.

We obtain multiple results for global rotations of the single cameras w.r.t. to the fused model. A single solution is found by single rotation averaging using a mean shift procedure. Furthermore, a „median camera“ is passed as initial camera to a following adjustment step, which employs the aforementioned structureless approach. The process is repeated until a single model has been adjusted. The process makes use of scene elements (3D points) only during initialization of triplet poses (Figure 8 and 9) to increase robustness in this stage. It remains free of these otherwise, making the approach rather insensitive to e.g. points at infinity or noisy structure estimation.

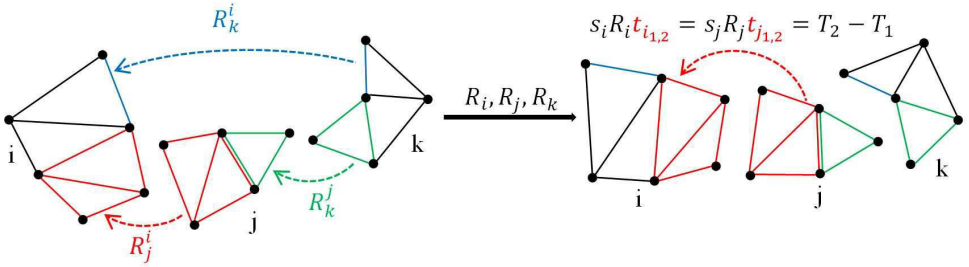

Figure 7: Relative rotations between submodels (left, lower / upper indices indicate source / target frame) sharing graph nodes (cameras) and edges (scaled relative translations between cameras). The following position registration (right) uses global submodel rotations (lower index only, global target frame omitted) and relative bases t between two cameras along with an unknown scale to estimate global positions T (here indicated only for one graph edge).

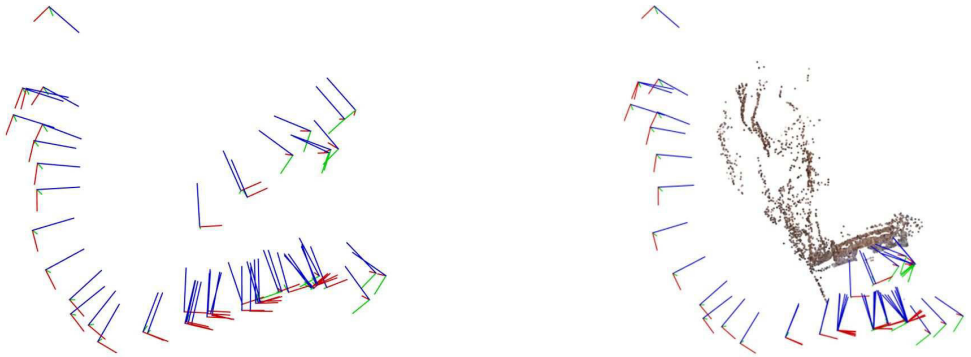

Figure 8: Starting solution after fusing triplets of a dataset (left), result final after adjustment (right). The RANSAC based triplet initialization significantly improves robustness against short baselines.

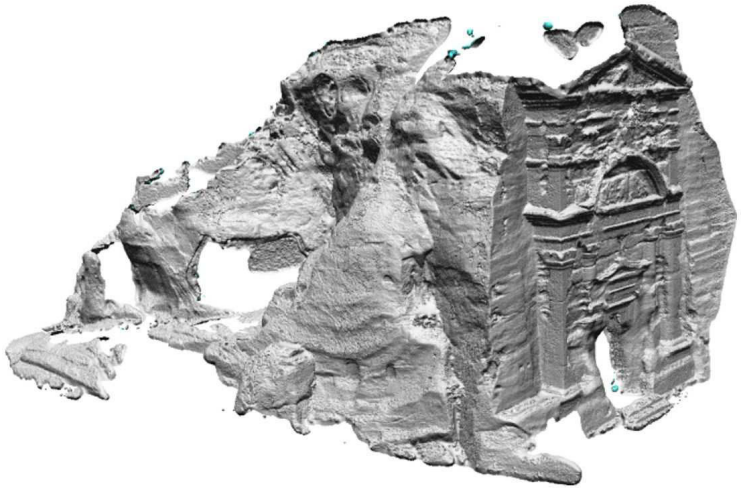

Figure 9: Mesh generated using SURE.

A Systematic Comparison of Direct and Image-Based Georeferencing in Challenging Urban Areas

Image-based mobile mapping systems enable an efficient acquisition of georeferenced image sequences, which can be used for geo-data capture in subsequent steps. In order to provide accurate measurements in a given reference frame while e.g. aiming at high fidelity 3D urban models, high quality georeferencing of the captured multi-view image sequences is required. Moreover, sub-pixel accurate orientations of these highly redundant image sequences are needed in order to optimally perform steps like dense multi-image matching as a prerequisite for 3D point cloud and mesh generation. While direct georeferencing of image-based mobile mapping data performs well in open areas, poor GNSS coverage in urban canyons aggravates fulfilling these high accuracy requirements. Hence, we conducted comprehensive investigations aiming at assessing the quality of directly georeferenced sensor orientations as well as the expected improvement by image-based georeferencing in a challenging urban environment in the city center of Basel, Switzerland (see Figure 10) Three street sections of this study area were mapped three times by the multi-sensor stereovision mobile mapping system of the Institute of Geomatics Engineering (IVGI), University of Applied Sciences and Arts Northwestern Switzerland (FHNW), once in July 2014 and twice during a day in August 2015. A NovAtel SPAN inertial navigation system that consists of a tactical grade inertial measurement unit and a L1/L2 GNSS kinematic antenna enabled direct georeferencing of the imagery captured approx. every meter. Even though multi-view images were acquired, our investigations focused on imagery from the main stereovision system facing forward, which features two 11 MP cameras and a calibrated stereo base of 905 mm.

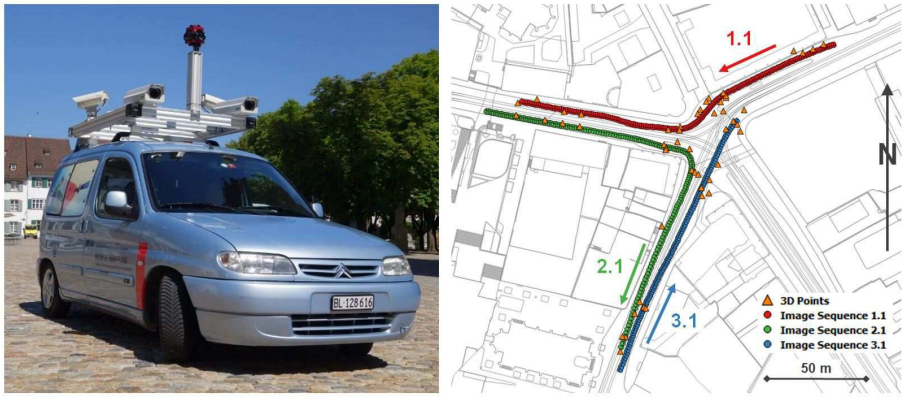

Figure 10: IVGI mobile mapping system with sensor configuration for the campaign in July 2014 (left) and base map of the study area with overlaid projection centers of selected stereo image sequences as well as 3D reference points (Source: Geodaten Kanton Basel-Stadt) (right).

For direct georeferencing, we processed navigation data in tightly coupled mode using the GNSS and inertial post-processing software Inertial Explorer from NovAtel. Image-based georeferencing results were generated using Agisoft PhotoScan by incorporating exterior orientation parameters from direct georeferencing as well as automatically determined image observations to tie points and manually defined image observations to approx. 20 ground control points per sequence in the bundle adjustment. Afterwards, we computed deviations of projection centers between direct and image-based georeferencing for all nine sequences (see Figure 11). These 3D deviations with a mean value of approx. 40 cm range from 46 to 803 mm and the height is the component with the largest residuals for all sequences but for 3.2. Trajectories of stereo image sequences captured on the same street section at different times show differences of up to several decimeters. While we obtained small deviations for sequences 1.1 and 2.0, they are significantly larger for the other sequences of these two street sections. Direct sensor orientations of stereo image sequences 3.1 und 3.2 were determined accurately, since all deviations lie in in the range of one decimeter.

While comparing 3D coordinates of camera trajectories both from direct georeferencing and bundle block adjustment gives some hints on the respective quality, accuracy investigations on 3D coordinates of measured image points are much more evident. For computation of these 3D coordinates by spatial intersection, orientation parameters from direct georeferencing and bundle adjustment can be used. Therefore, we established several groups of two, three or four ground control points (GCP) and defined approx. half of the previously used GCP as check points. Then, we computed check point residuals for two scenarios. First, only one GCP group at each end of a segment was defined. Second, two additional GCP groups in-between and close to the corresponding sharp curve were established. For scenario one with two GCP groups, we obtained

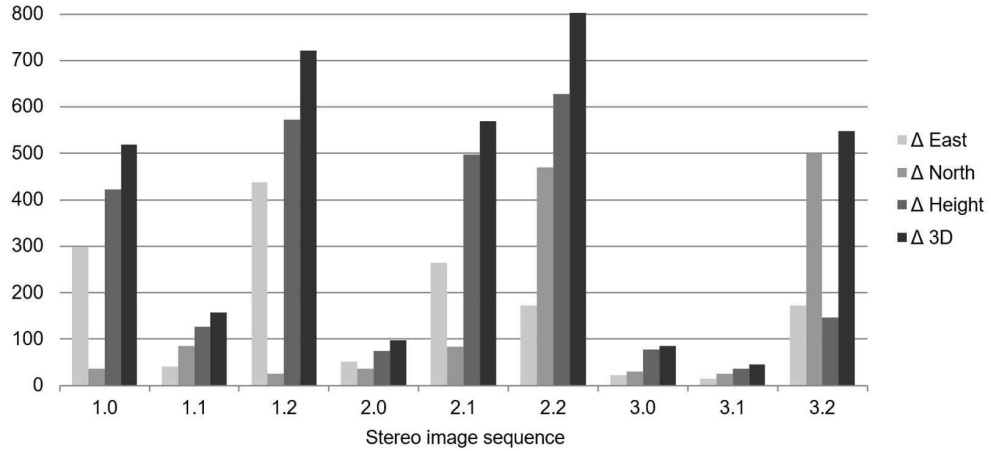

Figure 11: RMSE values in mm for deviations of projection centers between direct and image-based georeferencing (stereo image sequence x.y where x corresponds to the street sections 1 to 3 shown in Figure 10 and y corresponds to the campaign, 0 = 24./27.7.2014, 1 = 20.8.2015 10:30-10:37, 2 = 20.8.2015 10:47-10:53).

mean check point residuals of around 15 cm which is roughly three times better than a value of approx. 40 cm for direct georeferencing (see Table 1). Scenario two featuring four GCP groups, which led to check point residuals per sequence of 21-73 mm, shows to improve the direct georeferencing accuracy by an order of magnitude.

Stereo image sequence	**Number of check points**	**Direct**	**Image-based 2 GCP groups**		**Image-based 4 GCP groups**	
		Δ3D [mm]	**Δ3D [mm]**	**Impr. factor**	**Δ3D [mm]**	**Impr. factor**
1.0	15	555	137	4.1	27	20.4
1.1	11	168	42	4.0	21	8.0
1.2	11	774	121	6.4	26	29.4
2.0	11	131	76	1.7	48	2.7
2.1	12	593	432	1.4	73	8.1
2.2	11	813	425	1.9	36	22.5
3.0	8	174	42	4.2		
3.1	10	64	30	2.1		
3.2	10	568	53	10.8		
Mean		**427**	**151**	**2.8**	**39**	**11.1**

Table 1: RMSE values for check point residuals of direct and image-based georeferencing

Photogrammetric Systems

Using UAS for efficient DTM update in national mapping

As it is already known quite some years unmanned aircraft systems (UAS) in combination with matured dense image matching algorithms may offer an efficient tool for the generation of 3D point clouds representing the local surface or terrain (DSM / DTM). This data can be used to update already existing digital surface/terrain model, as they are used in national mapping and already provided nation-wide. The existing nation-wide terrain models typically are derived from manned airborne laser scanning flight campaigns. Especially when there are changes in terrain, which normally are caused by larger infrastructure projects, updating the old DTM is required. UAS may now offer an option to flexible map those changes almost immediately.

UAV-based laser systems are available meanwhile, which would allow the similar data scenario as for the original DTM manned aircraft acquisition, but their systems availability is quite limited until now. Furthermore these systems are not available in the below $<$ 10kg maximum-take-of-weight class which prevents flexible usage (because of extra effort to get permission to fly) and also will be quite costly. This is why dense image matching is a favored approach used in UAS to get dense surface point clouds.

In order to get the data most efficiently, the effort in additional control point measurement and targeting has to be minimized. Some of the UAS-platform providers claim to obtain the 3D point clouds from imagery georeferenced within GNSS-supported bundle adjustment without usage of any ground control. This for sure would be the most efficient way of DTM generation and is of interest for many users, including the national mapping agencies. This is why the LGL Baden-Württemberg (LGL BW) has investigated in the performance of DTM updating using UAS-based ground control free georeferenced imagery.

The test was done in a road construction area using the MAVinci Sirius Pro UA-System. Images were taken under operational conditions with a ground pixel size (GSD) of 3cm. Because of the extension of the area the block was split into two overlapping image blocks. It was requested by LGL BW to finally derive the 3D point clouds with a single point accuracy better than 10cm. GNSS data have been captured within the unmanned aircraft vehicle (UAV) and on a reference station placed in / close to the area of interest. Additional check points, a vertical profile captured by kinematic road survey and the reference DTM from traditional airborne laser scanning was used for independent performance checking. The georeferencing and point cloud generation has been done with two different software tools to allow double checks.

The performance from check point analysis is given in Figure 12. 13 points are available; the differences reflect the absolute quality (accuracy) of 3D single point determination. The std.dev. are consistent and well within the 1 GSD range: about 2.5cm for horizontal (east / north), and 3.3cm for vertical axis - still in the vertical differences an additional constant offset of about 7.5cm is present, which might be due to some non-correctly calibrated system parameter.

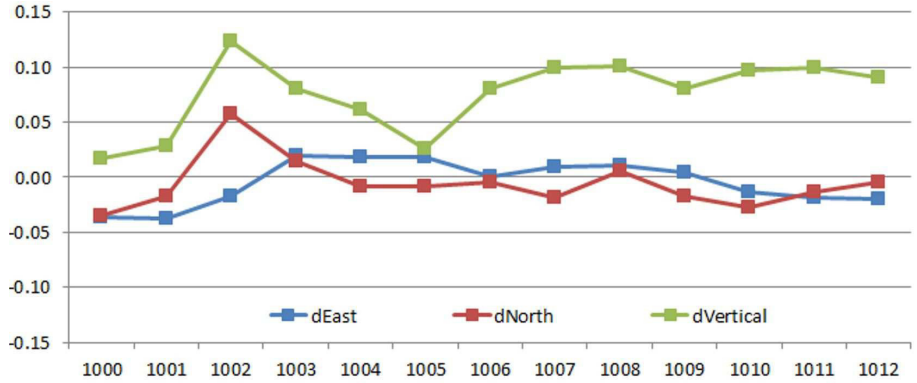

Figure 12: Check point differences [m] at 13 independent check points. These differences reflect the accuracy of 3D point positioning.

In Figure 13 the vertical differences from the road profile obtained from mobile mapping are shown. The individual in the diameter of each circle reflects the size of the difference between height from UAS-based point cloud and reference height from kinematic road survey. The std.dev. is about 5cm quite similar to the performance from single check point differences. Again, a systematic offset in height is visible. Interesting to note, that differences are bigger, where there are trees and more steep terrain. As this should not be expected in the UAS-based point cloud generation this most likely is due to less accurate kinematic vertical check points. The kinematic GNSS road survey might have been influenced by satellite occlusions here.

Finally the UAS based surface model is compared to the already available terrain model from airborne laser scanning. These differences are shown in Figure 14. As the surface model is „higher“ than the underlying terrain the differences (DSM minus DTM) are all positive - for most of the areas, as most of them are with vegetation. The vegetation is included in this difference. Still, the change in terrain caused by the infrastructure work is clearly visible.

As it was shown from the study, the use of precise GNSS-trajectory allows for the control point free evaluation of UAS-data. This in principle was known from large format photogrammetric airborne image flights, still it is interesting to see, that it now works in UAS environment - even in combination with quite cheap camera, not primarily designed for photogrammetric purpose. The 3D point cloud is obtained within the required accuracy better than 10cm accuracy. The image based derived surface model was filtered and then used to locally update the existing DTM from national mapping. Still, remaining systematic offsets cannot be detected without any external reference. Nevertheless, as within this system a GNSS-reference station is used close or inside the test area, this single point is enough to completely correct for any systematic offset.

Figure 13: Quality circles depicting the vertical accuracy. The diameter of every circle reflects the quality of height determination (see legend). The reference heights are derived from a kinematic GNSS survey of the road profile.

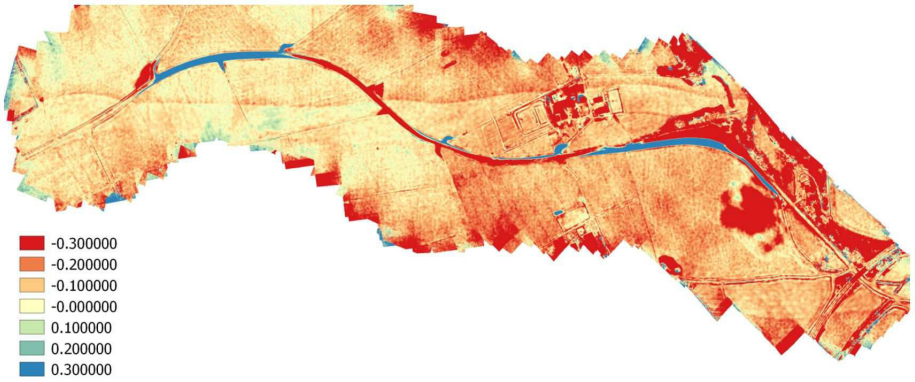

Figure 14: Height differences [m]. The color coding reflects the size of the difference (see legend). As the difference is computed as DTM minus DSM the differences are mostly positive. The effect of vegetation is clearly visible and has to be filtered in order to reduce the DSM to the DTM (if necessary). Also notice the systematic „snake like“ lines in the upper and lower part of the difference plot. They indicated differences due to small errors from the strip alignment in the processing of the DTM derived from standard airborne laser scanning. This additionally proves the high local accuracy and consistency of the image based UAS point clouds.

Modified Epipolar Resampling and Orientation Method for Satellite Imagery

Nowadays, high resolution satellite images have been commonly used for the point cloud and Digital Surface Model (DSM) generation or 3D reconstruction. Since we already have a completely workflow to process the satellite imagery, we focus more on the improvement of the pipeline.

New epipolar model

In order to get very dense point cloud, the modified Semi-Global Matching (tSGM) method is an efficient tool. Because the epipolar images will reduce the search range from 2D space to 1D space and largely decrease the processing time, epipolar resampling is required before the dense matching. As we know, the epipolar geometry of satellite pushbroom sensors only exists in small range area, and the epipolar curve is more like hyperbola line than straight line. Many applications only carry out the epipolar resampling in small tiles.

The present work aims at the epipolar resampling for the whole image without tiling. In our method, each epipolar curve is approximated by several segments. In order to get a proper epipolar segment length, we use the height range calculated from RPCs to define it. The sketch of the method is shown in Figure 15, and the main steps are:

- ▷ Select the points on the border as the start point and calculate its epipolar line function.
- ▷ Define the epipolar segment length and end point.
- ▷ Resample original image along the epipolar segment until it reach the end points.
- ▷ Then choose the end point as the start point to derive new epipolar segments.
- ▷ Repeat this procedure till reach the other border of the image.

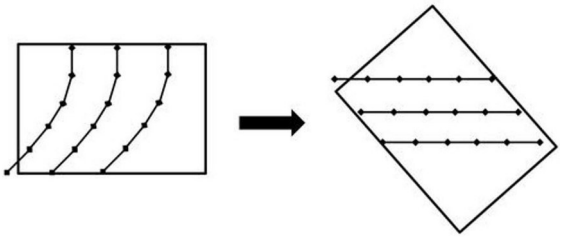

Figure 15: Epipolar curve approximation and resampling.

All these steps are implemented with RPC projection trajectory method, and some evaluations have been done on a QuickBird data covers Melbourne. Twenty-five pairs of check points are selected to calculate the vertical parallaxes. The result is shown in Figure 16, all vertical parallaxes are smaller than 1 pixel and the root-mean-square (RMS) error is 0.499 pixels. This indicates that the piece-wise epipolar resampling method can reach sub-pixel level.

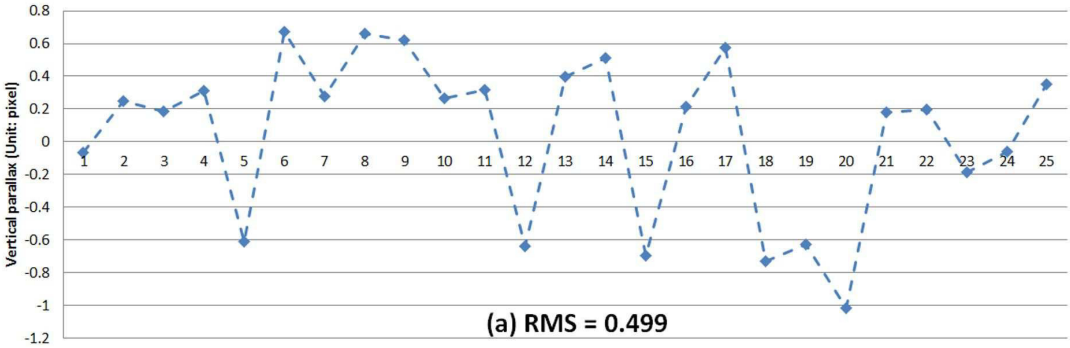

Figure 16: Vertical parallaxes of QuickBird Melbourne dataset.

Relative orientation without ground controls

From our experience, the Rational Polynomial Coefficients (RPCs) provided by the vendor are not always accurate enough. The corresponding points on matching image might not locate on the corresponding epipolar curve because of the lack of RPCs precision. Moreover, users might not have ground control information for bundle block adjustment. Therefore, relative orientation is an important pre-procedure to generate high quality epipolar geometry. Some researches use an error vector to compensate the error in matching image space, but only for small tiles.

The present work introduces a relative orientation method for entire satellite images without tiling. This method doesn't need ground control information, but only use the tie points and rough RPCs. The tie points are generated half-automatically with software ENVI, and their accuracy are considered as sub-pixel level. The method measures the difference between corresponding points and corresponding epipolar curves on the matching image. Then we estimate an affine model as a global correction to compensate the location error for the whole image. Twenty-four check points are selected from the Pleiades imagery to verify the quality of this global compensated relative orientation. Before processing, the location error is as large as ca. 10 pixels. And after the orientation, the location error is less than 1 pixel. The result is shown in Figure 17. According to the experiments, proposed relative orientation method can achieve sub-pixel accuracy and provide a good geometry for following epipolar resampling.

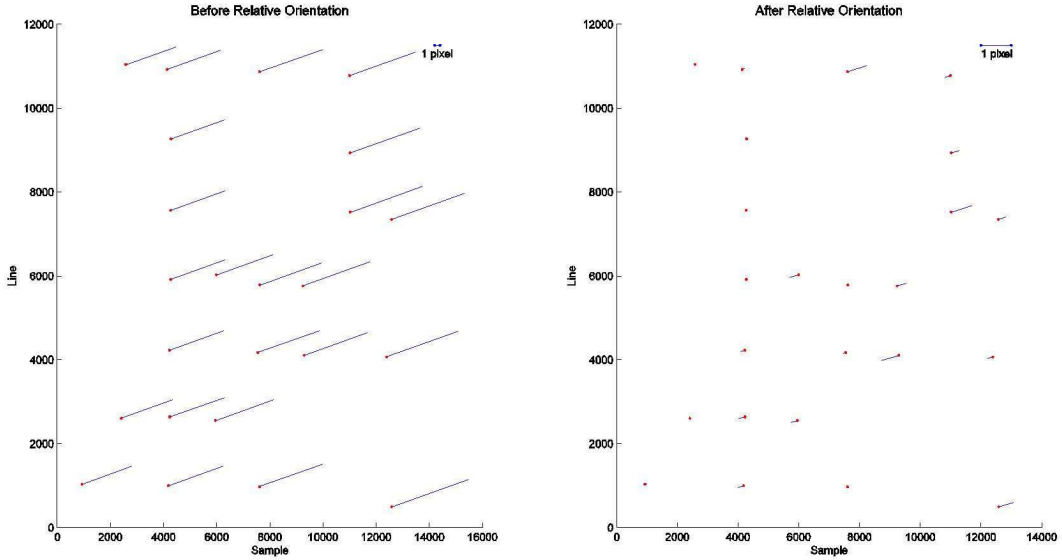

Figure 17: Location error of Pleiades Taibei dataset (The red point are the true corresponding points' location, blue lines are the distance between true location and the epipolar curve. The scale of the distance is shown in the right top of the figure).

Remote Sensing

4D Change Detection based on Persistent Scatterer Interferometry (4DCDPSI)

Persistent Scatterer Interferometry (PSI) detects and analyses PS points, which are characterized by strong, stable, and coherent radar signals throughout a time series of SAR images. Attributes of PS points, such as line-of-sight velocities (mm/year level) and topography height, can be derived and used for topography reconstruction and deformation analysis over a scene of interest. In practice, PSI works particularly well in monitoring built-up cities because densely clustered PS points are anticipated to be detected from stationary buildings.

A prerequisite of forming PS points is that their signals throughout time-series SAR images must maintain coherence. To avoid coherence loss, a scene of interest covered with PS points is modelled to be steady and free of any big changes. A typical example is a building containing PS-like substructures stays unchanged over the acquisition period of an SAR image stack. Therefore, the local PS points can be extracted for further analysis. In contrast, if the substructures disappear due

to construction, the local PS candidates are discarded in the initial screening of a standard PSI processing for dominant and temporally stable scatterers. In other words, big change information is unobtainable in PSI.

In this study, we propose 4D change detection based on PSI to detect disappearing and emerging PS points (3D) along with their occurrence times (1D). We define these two point types as disappearing big change (DBC) and emerging big change (EBC) points considering that they are subject to big changes. At first, multi-temporal SAR images are divided into several image subsets by a time series of break dates. For each pixel, the phases in the image subsets are adopted to determine its temporal coherences via a standard PSI processing. The temporal coherence reflects the phase stability and is used as an indicator of a PS point. Based on this concept, we introduce a sequence of change indices for each pixel, which are computed from its temporal coherences, to quantify its probability of being a DBC or EBC point at different times. All pixels' change indices are used to design a global and automatic thresholding method to extract DBC and EBC points. Then, the disappearance date of each DBC is detected from the break dates based on the temporal variation in its change index sequence; the same process is also applied to each EBC point to determine its emergence date.

By using a stack of TerraSAR-X images, the real data test successfully detects the disappearing and emerging buildings in Berlin, Germany. One example (Figure 18) demonstrates construction monitoring of single high-rise buildings. The left building's main structure (area 1) had been erected in early 2013 and the remaining substructures were later complemented over time. In area 2, certain new storeys were built upon an existing building from low to high level in sequence along the magenta arrow. This example shows that our technique is able to provide detailed spatiotemporal information about construction progress.

Band Co-registration of Miniature Multi-lens Multispectral Cameras

Miniature multi-lens multispectral cameras (Minim-MSCs) can acquire discrete spectral bands by separated lenses and filters. However, the acquired original multispectral images have significant band misregistration errors due to the lens distortion, and the positions as well as viewing angles of each lens are different. In order to obtain band co-registered multispectral imagery for remote sensing applications, the modified projective transformation (MPT) is adopted for transferring multiple images geometry of a multi-lens imaging system into one sensor geometry, and together with a robust and adaptive correction (RAC) procedure for correcting serval systematic errors after MPT.

Equation (1) and (2) are the mathematical forms of MPT. The (x_o, y_o) and (x_{mpt}, y_{mpt}) are the image coordinates of original image sensor and after MPT, respectively. The $m_{11} \sim m_{33}$ are elements of rotation matrix between the reference image sensor and the others. The (Δx,Δy) are lens distortion corrections of each image sensor. The f_o and f represent the focal length of the original image sensor and the focal length of co-registered image, respectively. As one image sensor is chosen as reference, the others can be transfer to the reference image plane through

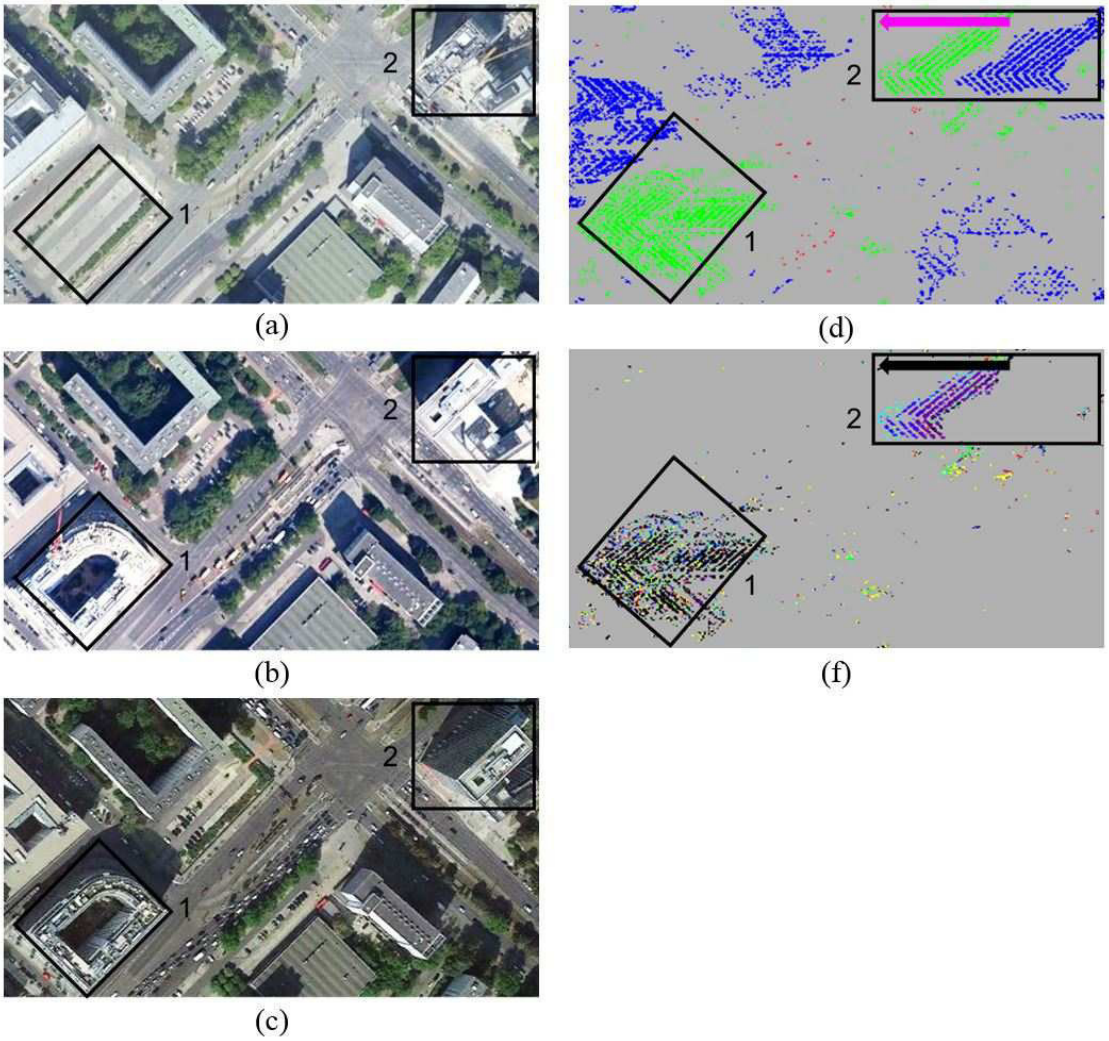

Figure 18: Construction monitoring of single high-rise buildings. Areas 1 and 2 are used for in-depth discussion. GE images were acquired on (a) September 12, 2010, (b) May 20, 2012, and (c) September 5, 2014. (d) Steady, disappearing, and emerging substructures represented by PS (blue), DBC (red), and EBC (green) points. (e) Disappearance and emergence dates: black to red, earliest to latest.

MPT that can correct the difference of lens distortion and viewing angles among lenses. Since some systematic errors still exist after MPT, the RAC is utilized to correct the remaining errors. As depicts in equation (3) and (4) are the functions of RAC that can correct the quadratic (SS_x, SS_y), linear (S_x, S_y), and displacement errors (d_x, d_y) in x and y directions.

Figure 19 shows the original multispectral images of three state-of-the-art Minim-MSCs, i.e. Tetracam MiniMCA-12, Micasense Rededge, and Parrot Sequoia, before and after band co-registration processing. It shows that the original multispectral images have significant lens distortion and ghosting effects, but those effects are both eliminated after applying the proposed band co-registration method. The band co-registration accuracy with and without RAC of three state-of-the-art Minim-MSCs are summarized in Figure 20, in which it summarized the mean, maximum (Max.), and minimum (Min.) values among different spectral band image matching pairs. In Figure 20, the label A, B, and C represent Tetracam MiniMCA-12, Micasense Rededge, and Parrot Sequoia, respectively. The A0, B0, and C0 are the results after MPT without further correction, in which A1, B1, and C1 are the results after applying the RAC. Experimental results show that the initial band co-registration results have an average accuracy range in 1.05 1.14 pixels, and were significantly improved to 0.29 0.37 pixels if RAC was applied.

$$x_{mpt} = -f\frac{m_{11}(x_o + \Delta x) + m_{21}(y_o + \Delta y) - f_o m_{31}}{m_{13}(x_o + \Delta x) + m_{23}(y_o + \Delta y) - f_o m_{33}} \quad (1)$$

$$y_{mpt} = -f\frac{m_{12}(x_s + \Delta x) + m_{22}(y_s + \Delta y) - f_o m_{32}}{m_{13}(x_s + \Delta x) + m_{23}(y_s + \Delta y) - f_o m_{33}} \quad (2)$$

$$\mathrm{x} = x_{mpt} + SS_x \times (\Delta x_{mpt})^2 + S_x \times \left(\Delta x_{mpt}\right) + d_x \quad (3)$$

$$y = y_{mpt} + SS_y \times (\Delta y_{mpt})^2 + S_y \times \left(\Delta y_{mpt}\right) + d_y \quad (4)$$

We can concluded that the proposed method can adaptively compensate the remaining systematic errors after MPT, which has benefits of robustness and accurate band co-registration accuracy that is suitable for various types of Minim-MSCs. In addition, the co-registered images can strengthen the ability of spectral analysis as we can obtain undistorted images for deriving various vegetation indices, and acquire accurate radiometric information since there is no blending pixels.

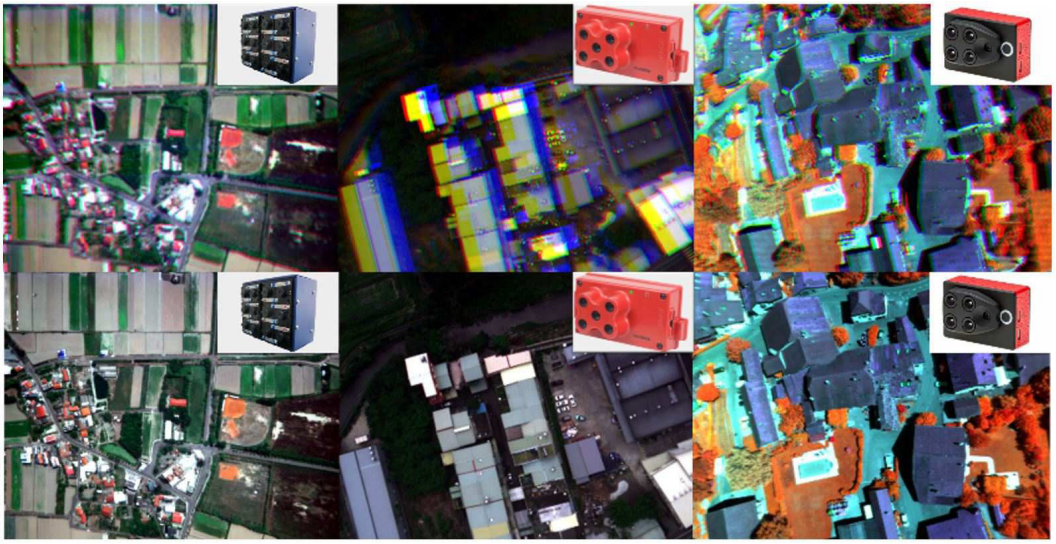

Figure 19: Original multispectral images before and after band co-registration. The images from left to right are Tetracam MiniMCA-12, Micasense Rededge, and Parrot Sequoia, which can obtain bands of 12, 5, and 4 multispectral images, respectively.

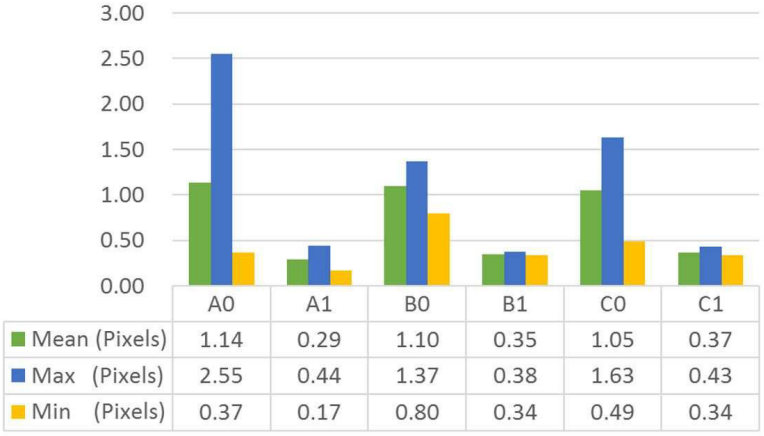

	A0	A1	B0	B1	C0	C1
Mean (Pixels)	1.14	0.29	1.10	0.35	1.05	0.37
Max (Pixels)	2.55	0.44	1.37	0.38	1.63	0.43
Min (Pixels)	0.37	0.17	0.80	0.34	0.49	0.34

Figure 20: Band co-registration accuracy of three state-of-the-art Minim-MSCs.

References 2016

Carboni, N., Bruseker, G., Guillem, A., Bellido Castañeda, D., Coughenour, C., Domajnko, M., de Kramer, M., Ramos Calles, M. M., Stathopoulou, E. K., Suma, R.: Data Provenance in Photogrammetry through Documentation Protocols. ISPRS Ann. Photogramm. Remote Sens. Spatial Inf. Sci., III-5, 57-64.

Cavegn, S., Haala, N.: Image-Based Mobile Mapping for 3D Urban Data Capture. Photogrammetric Engineering, Remote Sensing Vol. 82, No. 12, December 2016, 925-933.

Cavegn, S., Nebiker, S., Haala, N.: A Systematic Comparison of Direct and Image-Based Georeferencing in Challenging Urban Areas. Int. Arch. Photogramm. Remote Sens. Spatial Inf. Sci., XLI-B1, 529-536.

Cefalu, A., Haala, N.,, Fritsch, D.: Structureless Bundle Adjustment with Self-Calibration Using Accumulated Constraints. ISPRS Ann. Photogramm. Remote Sens. Spatial Inf. Sci., III-3, 3-9.

Cramer, M., Leinss, B.: Welche ist am besten? - Anmerkungen zur Auswahl von Kamerasystemen in der UAS-Luftbildphotogrammetrie. DVW-Seminar „UAV 2016 - Vermessung mit unbemannten Flugsystemen“, at Bonn, Germany, Volume: Schriftreihe des DVW, Volume 82 / 2016, 97-118.

Gong, K., Fritsch, D.: A Detailed Study About Digital Surface Model Generation Using High Resolution Satellite Stereo Imagery. ISPRS Ann. Photogramm. Remote Sens. Spatial Inf. Sci., III-1, 69-76.

Haala, N., Cavegn, S.: High Density Aerial Image Matching: State-of-the-Art and Future Prospects. Int. Arch. Photogramm. Remote Sens. Spatial Inf. Sci., XLI-B4, 625-630.

Kenduiywo, B. K., Bargiel, D., Soergel, U.: Crop Type Mapping from a Sequence of TerraSAR-X Images with Dynamic Conditional Random Fields. ISPRS Ann. Photogramm. Remote Sens. Spatial Inf. Sci., III-7, 59-66.

Kraft, T., Geßner, M., Meißner, H., Cramer, M., Gerke, M., Przybilla, H. J.: Evaluation of Metric Camera System Tailored for High Precision UAV Applications. Int. Arch. Photogramm. Remote Sens. Spatial Inf. Sci., XLI-B1, 901-907.

Niemeyer, J., Rottensteiner, F., Soergel, U., Heipke, C.: Hierarchical Higher Order CRF for the Classification of Airborne Lidar Point Clouds in Urban Areas. Int. Arch. Photogramm. Remote Sens. Spatial Inf. Sci., XLI-B3, 655-662.

Rothermel, M., Haala, N., Fritsch, D.: A Median-Based Depthmap Fusion Strategy for the Generation of Points. ISPRS Ann. Photogramm. Remote Sens. Spatial Inf. Sci., III-3, 115-122.

Schack, L., Soergel, U., Heipke, C.: Graph Matching for the Registration of Persistent Scatters to Optical Oblique Imagery. ISPRS Ann. Photogramm. Remote Sens. Spatial Inf. Sci., III-7, 195-202.

Schmidt, A., Kruse, C., Rottensteiner, F., Soergel, U., Heipke, C.: Network Detection in Raster Data Using Marked Point Processes. Int. Arch. Photogramm. Remote Sens. Spatial Inf. Sci., XLI-B3, 701-708.

Schunert, A., Soergel, U.: Assignment of Persistent Scatterers to Buildings. In: IEEE Transactions on Geoscience and Remote Sensing, ISSN 0196-2892, Volume 54, Issue 6, 3116-3127.

Soergel, U., Wegner, J. D., Thiele, A.: Fusion von optischen und Radardaten. In Band Photogrammetrie und Fernerkundung, Christian Heipke (Ed.) - Handbuch der Geodäsie, 6 Bände, Willi Freeden, Reiner Rummel (Eds.). Springer Berlin Heidelberg,

Tutzauer, P., Becker, S., Fritsch, D., Niese, T., Deussen, O.: A Study of the Human Comprehension of Building Categories Based on Different 3D Building Representations. Photogrammetrie-Fernerkundung-Geoinformation, 2016(5-6), 319-333.

Tutzauer, P., Becker, S., Niese, T., Deussen, O., Fritsch, D.: Understanding Human Perception of Building Categories in Virtual 3D Cities - A User Study. Int. Arch. Photogramm. Remote Sens. Spatial Inf. Sci., XLI-B2, 683-687.

Walter, V., Laupheimer, D., Fritsch, D.: Use and Optimization of Paid Crowdsourcing for the Collection of Geodata. Int. Arch. Photogramm. Remote Sens. Spatial Inf. Sci., XLI-B4, 253-257.

Yang, C. H., Kenduiywo, B. K., Soergel, U.: Change Detection Based on Persistent Scatterer Interferometry - A New Method of Monitoring Building Changes. ISPRS Ann. Photogramm. Remote Sens. Spatial Inf. Sci., III-7, 243-250.

Dissertations

Khosravani, Ali Mohammad: Automatic Modeling of Building Ineriors Using Low-Cost Sensor Systems. Deutsche Geodätische Kommission, Reihe C, Nr. 767, München 2016, ISBN 978-3-7696-5179-9, 132 S. (Softcopy only).

Peter, Michael: Crowd-sourced Reconstruction of Building Interiors. Deutsche Geodätische Kommission, Reihe C, Nr. 768, München 2016, ISBN 978-3-7696-5180-5, 145 S. (Softcopy only).

Rothermel, Matthias: Development of a SGM-Based Multi-View Reconstruction Framework for Aerial Imagery. Reihe C, Nr. 792, München 2016, ISBN 978-3-7696-5204-8, 115 S. (Softcopy only).

Wenzel, Konrad: Dense Image Matching for Close Range Photogrammtery. To be published at Deutsche Geodätische Kommission.

Master Theses

Almassri, H.: Detection of Repetitive Parking Lot Boundaries for Near Range Camera Systems. Supervisors: Tranzer, M. (Robert Bosch GmbH), Haala, N.

Arinita, D.: Detecting 3D Building Symmetries - an Empirical Study. Supervisors: Becker, S., Cramer, M.

Berdanoglu, C.: Extraction of Vectorial Information and Accuracy Analysis of Railway Mapping. Supervisors: Fritsch, D., Becker, S.

Burlacu, D. M.: Tie point extraction in UAS imagery for vegetation areas. Supervisor: Cramer, M.

Feng, B.: Digital Preservation of Calw Altburgerstrasse by Means of Automated HDS and Photogrammetric Texture Mapping. Supervisors: Balsa-Barreiro, J., Fritsch, D.

Han, M.: Präsentation photogrammetrischer Daten in Virtual Reality Umgebungen. Supervisor: Tutzauer, P.

Kappel, F.: Traffic Sign Detection and Classification using Deep Learning. Supervisors: Liu, F. (Volvo Car Corporation), Haala, N.

Keshtkarrezaei, R.: Performance Test of Open-Source SLAM for Indoor Navigation. Supervisors: Rudolph, T. (Aibotix), Haala, N.

Koirala, B.: Image Rectification to Improve Tie Point Matching in Mobile Mapping Applications. Supervisor: Haala, N.

Nehaichik, A.: Verfahren zur Detektion dynamischer Marker und Unterstützung der Landung von Multikoptern. Supervisors: Segor, F. (Fraunhofer-Institut für Optronik, Systemtechnik und Bildauswertung), Haala, N.

Poudel, D.: Development of Graphical User Interface to visualize the Quality of digitized Polygons. Supervisor: Walter, V.

Szatkowska, M.: Analysis of Distortion Parameters for Physical Interpretation of Intrinsic Camera Alignment. Supervisors: Apel, U. (Robert Bosch GmbH), Küver, M. (Robert Bosch GmbH), Haala, N.

Wang, S.: Comparison of Different Transformations of Direct Georeferencing in National Coordinates. Supervisor: Cramer, M.

Wang, T.: Development of an Algorithm for Ghost Detection in the Context of Stray Light Test. Supervisors: Apel, U. (Robert Bosch GmbH), Haala, N.

Zhang, W.: Schwarmbasierte Lokalisierung auf dem Parkplatz mittels GraphSLAM. Supervisors: Schuster, F. (Daimler AG), Haala, N.

Bachelor Theses

Hajer, L.: Voxelbasierte Flugplanung für die photogrammetrische Fassadenerfassung mittels Multikopter. Supervisors: Cefalu, A., Haala, N.

Kölle, M.: Automatische Erkennung und Klassifikation von Karten mittels Methoden der Bildverarbeitung. Supervisors: Walter, V., Haala, N.

Sabow, F.: Direkte Georeferenzierung von UAV-Anwendungen. Supervisors: Cramer, M., Haala, N.

Li, Y.: Voxelbasierte Extraktion von Vegetation aus photogrammetrischen 3D-Punktwolken. Supervisors: Becker, S., Haala, N.

Preuss, S.: Aufbau und Durchführung eines Nutzertests zur Klassifikation von 3D Gebäuden in einer virtuellen 3D Umgebung. Supervisors: Becker, S., Patrick Tutzauer

Stilling, N.: Qualitätsbewertung von heterogenen raumbezogenen Daten. Supervisor: Walter, V.

Straub, J.: Untersuchung bildbasierter Verfahren zur Analyse simulierter unterirdischer Massenbewegungen. Supervisor: Cefalu, A.

Usche, T.: Untersuchung von Softwarepaketen zur bildbasierten Rekonstruktion eines historischen Kraftfahrzeugs. Supervisor: Haala, N.

Xiao, M.: Superweitwinkel- und Fisheye-Kameras in photogrammetrischen Anwendungen. Supervisors: Cramer, M., Haala, N.

Activities in National and International Organizations

Cramer, M.:
Co-Chair ISPRS WG I/9: Integrated Sensor Orientation, Calibration, Navigation and Mapping

Englich, M.:
Webmaster ISPRS

Haala, N.:
Chair ISPRS WG II/2: Point Cloud Beneration
Vorsitz DGPF Arbeitskreis Sensorik und Plattformen

Sörgel, U.:
Vice President German Society for Photogrammetry, Remote Sensing and Geoinformation (DGPF)
Chair ISPRS WG III/3: SAR-Based Surface Generation and Deformation Monitoring

Walter, V.:
Member Editorial Advisory Board ISPRS Journal of Photogrammetry and Remote Sensing
National Correspondent of the ISPRS Commission IV

Education - Lectures/Exercises/Training/Seminars

Bachelor „Geodäsie und Geoinformatik“

Geoinformatics I (Walter)	2/2/0/0
Geoinformatics II (Walter)	1/1/0/0
Image Processing (Haala)	2/1/0/0
Integrated Fieldworks (Haala, Keller, Kleusberg, Sneeuw)	0/0/4/0
Introduction into Geodesy and Geoinformatics (Cramer, Keller, Kleusberg, Sörgel, Sneeuw)	4/2/0/0
Photogrammetry (Cramer)	2/1/0/0
Remote Sensing (Sörgel)	2/1/0/0
Signal Processing (Sörgel)	2/1/0/0
Urban Planning (Dvorak)	2/0/0/0

Master Course „Geodäsie und Geoinformatik“

Aerotriangulation (Cramer)	1/1/0/0
Computational Geometry (Walter)	1/1/0/0
Computer Vision for Image-based Acquisition of Geodata (Haala)	1/1/0/0
Databases and Geographical Information Systems (Walter)	1/1/0/0
Digital Terrain Models (Haala)	1/1/0/0
Fundamentals in Urban Planning (Dvorak)	2/0/0/0
Georeferencing of photogrammetric Systems (Cramer)	1/1/0/0
Modelling and Visualisation (Haala)	1/1/0/0
Pattern Recognition and Image Understanding (Haala)	1/1/0/0
Remote Sensing (Sörgel)	1/1/0/0
Scientific Presentation Seminar (Haala)	0/0/0/2
Topology and Optimisation (Becker)	1/1/0/0
Web-based GIS (Walter)	1/1/0/0

Master Course GEOENGINE

Airborne Data Acquisition (Cramer)	2/1/0/0
Geoinformatics (Walter)	2/2/0/0
Signal Processing (Sörgel)	2/1/0/0
Image-based Data Collection (Haala, Cramer)	2/1/0/0
Integrated Fieldworks (Haala, Sneeuw, Keller, Kleusberg)	0/0/4/0
Remote Sensing (Sörgel)	2/1/0/0
Topology and Optimisation (Becker)	2/1/0/0

Master Course „Infrastructure Planning“

Introduction to GIS (Walter)	2/0/0/0

Master Course „Aerospace Engineering“

Introduction into projective Geometry (Cramer)	2/0/0/0